

On the mechanism of open-flavor strong decays

E. S. Ackleh* and T. Barnes

*Computational and Theoretical Physics Group, Oak Ridge National Laboratory, Oak Ridge, Tennessee 37831-6373
and Department of Physics and Astronomy, University of Tennessee, Knoxville, Tennessee 37996-1200*

E. S. Swanson

Department of Physics, North Carolina State University, Raleigh, North Carolina 27695-8202

(Received 22 April 1996; revised manuscript received 5 August 1996)

Open-flavor strong decays are mediated by $q\bar{q}$ pair production, which is known to occur dominantly with 3P_0 quantum numbers. The relation of the phenomenological 3P_0 model of these decays to “microscopic” QCD decay mechanisms has never been established clearly. In this paper we investigate $q\bar{q}$ meson decay amplitudes assuming pair production from the scalar confining interaction (sKs) and from one gluon exchange (OGE). sKs pair production predicts decay amplitudes of approximately the correct magnitude and D/S amplitude ratios in $b_1 \rightarrow \omega\pi$ and $a_1 \rightarrow \rho\pi$ which are close to experiment. The OGE decay amplitude is found to be subdominant in most cases, a notable exception being ${}^3P_0 \rightarrow {}^1S_0 + {}^1S_0$. The full $sKs + \text{OGE}$ amplitudes differ significantly from 3P_0 model predictions in some channels and can be distinguished experimentally, for example, through an accurate comparison of the D/S amplitude ratios in $b_1 \rightarrow \omega\pi$ and $a_1 \rightarrow \rho\pi$. [S0556-2821(96)04121-5]

PACS number(s): 12.39.Jh, 13.25.-k

I. INTRODUCTION

Strong decays constitute a rather poorly understood area of hadronic physics. This is unfortunate because decay widths comprise a large portion of our knowledge of the strong interactions. Furthermore, strong couplings are expected to play an important role in many topics of current interest. For example, the discovery and interpretation of QCD exotica such as glueballs will depend on a sound understanding of the mixing of these states with nearby quarkonia.

Attempts at modeling strong decays date from Micu’s suggestion [1] that hadron decay proceeds through $q\bar{q}$ pair production with vacuum quantum numbers, $J^{PC} = 0^{++}$. Since this corresponds to a 3P_0 $q\bar{q}$ state, it is now generally referred to as the 3P_0 decay model. This suggestion was developed and applied extensively by Le Yaouanc *et al.* [2] in the 1970s. Studies of hadron decays using the 3P_0 model have been concerned almost exclusively with numerical predictions, and have not led to any fundamental modifications to the original model. Recent studies have considered changes in the spatial dependence of the pair production amplitude as a function of quark coordinates [3–6], but the fundamental decay mechanism is usually not addressed; this is widely believed to be a nonperturbative process, involving “flux tube breaking.” There have been some studies of the decay mechanism which consider an alternative phenomenological model in which the $q\bar{q}$ pair is produced with 3S_1 quantum numbers [7]; this possibility,

however, appears to disagree with experiment [4].

The goal of this paper is to explore possible microscopic models for hadronic decays. The constituent quark model is typically motivated by a nonrelativistic reduction of the one gluon exchange amplitude supplemented by a linear confinement term. The Lorentz structure of the confinement term is unknown *a priori*; however, comparison with spin splittings in the $c\bar{c}$ spectrum [8] and lattice gauge calculations [9] indicate that the confinement current is a Lorentz scalar. Our approach is to assume this Lorentz structure and nonrelativistic quark model parameters, and derive a set of effective quark pair creation operators, assuming as in field theory that the same interaction that causes scattering also leads to pair production. The matrix elements of these operators are completely determined in the nonrelativistic quark model; thus, we have absolute predictions of hadronic widths.

The remainder of this paper is arranged as follows. We first review the phenomenological 3P_0 model and its predictions, and a diagrammatic method for evaluating decay amplitudes is introduced. Candidate QCD-motivated quark model decay mechanisms are presented in Sec. III and the associated predictions are compared with experiment and the 3P_0 model. The summary and conclusions are followed by Appendixes which detail the diagrammatic method employed throughout this work.

II. SUMMARY OF THE 3P_0 MODEL

The 3P_0 pair production Hamiltonian for the decay of a $q\bar{q}$ meson A to mesons $B + C$ is usually written in a rather complicated form with explicit wave functions [3–6], which in the conventions of Geiger and Swanson [4] (to within an irrelevant overall phase) is

*Current address: Hewlett-Packard Corporation, SIT-UNIX Team, M.S.906-SE3, 20 Perimeter Summit Blvd., Atlanta, GA 30319-1417.

$$\begin{aligned}
\langle BC|H_I|A\rangle &= \gamma \int \int \frac{d^3r d^3y}{(2\pi)^{3/2}} e^{i\vec{P}_B \cdot \vec{r}} \Psi_A(\vec{r}) \langle \vec{\sigma} \rangle_{q\bar{q}} \cdot (i\vec{\nabla}_B \\
&\quad + i\vec{\nabla}_C + \vec{P}_B) \Psi_B^* \left(\frac{\vec{r}}{2} + \vec{y} \right) \Psi_C^* \left(\frac{\vec{r}}{2} - \vec{y} \right) \\
&\quad \times \delta(\vec{P}_A - \vec{P}_B - \vec{P}_C)
\end{aligned} \tag{1}$$

for equal quark and antiquark masses. The strength γ of the decay interaction is regarded as a free constant and is fitted to the data.

An equivalent formulation of the 3P_0 model regards the decays as due to an interaction Hamiltonian involving Dirac quark fields:

$$H_I = g \int d^3x \bar{\psi} \psi, \tag{2}$$

which in the nonrelativistic limit gives matrix elements identical to Eq. (1) with the identification

$$\gamma = \frac{g}{2m_q}, \tag{3}$$

where m_q is the mass of both produced quarks. Note that the operator $g\bar{\psi}\psi$ leads to the decay $(q\bar{q})_A \rightarrow (q\bar{q})_B + (q\bar{q})_C$ through the $b^\dagger d^\dagger$ term.

This model makes no reference to color, which if included would simply change the definition of the interaction strength γ ; since γ is fitted to the data, this would not change the predictions for meson decays. An *ad hoc* feature of the 3P_0 model is to allow only diagrams in which the $q\bar{q}$ pair separate into different final hadrons. This was originally motivated by experiment (specifically the weakness of $\phi \rightarrow \rho\pi$); in the QCD-based current-current decay models that we shall discuss subsequently, the absence of these hair-pin diagrams is a natural consequence of the production of the $q\bar{q}$ pair in a color octet state.

To determine a decay rate, we evaluate the matrix element of the decay Hamiltonian, which is of the form

$$\langle BC|H_I|A\rangle = h_{fi} \delta(\vec{A} - \vec{B} - \vec{C}). \tag{4}$$

This h_{fi} decay amplitude can be combined with relativistic phase space to give the differential decay rate, which is

$$\frac{d\Gamma_{A \rightarrow BC}}{d\Omega} = 2\pi \frac{PE_B E_C}{M_A} |h_{fi}|^2, \tag{5}$$

where we have set $\vec{A} = \vec{0}$ and $P = |\vec{B}| = |\vec{C}|$. An equivalent result is quoted by Geiger and Swanson [4] as the ‘‘actual phase space’’ case of their Eq. (20). We shall usually quote results for the amplitude $\mathcal{M}_{L_{BC}S_{BC}}$, defined by

$$\Gamma_{A \rightarrow BC} = 2\pi \frac{PE_B E_C}{M_A} \sum_{LS} |\mathcal{M}_{LS}|^2. \tag{6}$$

For $S=0$ this \mathcal{M}_{LS} is the coefficient of Y_{LM} in h_{fi} , and in general is the amplitude $\langle JM(L_{BC}, S_{BC})|BC\rangle$ in the BC final state.

We have developed a diagrammatic technique for evaluating the h_{fi} matrix element. This is discussed in detail for $\rho \rightarrow \pi\pi$ in the 3P_0 model in Appendix A.

A. 3P_0 model decay rates for light $L_{q\bar{q}}=0$ and $L_{q\bar{q}}=1$ mesons

Since the 3P_0 model involves a free phenomenological interaction strength γ , comparison with experiment requires a fit to several rates (to determine both γ and the wave function parameters) or a determination of amplitude ratios in decays with more than one partial wave, in which γ cancels. Here we illustrate both applications; first we will evaluate the dominant two-body decay rates of light nonstrange mesons with $L_{q\bar{q}}=0$ and $L_{q\bar{q}}=1$, and subsequently we will evaluate D/S ratios in the decays $b_1 \rightarrow \omega\pi$, $a_1 \rightarrow \rho\pi$, and $h_1 \rightarrow \rho\pi$.

An \mathcal{M}_{LS} decay amplitude in the 3P_0 model with simple harmonic oscillator (SHO) wave functions is proportional to a polynomial $\mathcal{P}_{LS}(x)$ in $x = P/\beta$ times an exponential,

$$\mathcal{M}_{LS} = \frac{\gamma}{\pi^{1/4} \beta^{1/2}} \mathcal{P}_{LS}(x) e^{-x^2/12}. \tag{7}$$

For the cases considered here these polynomials are

$$\mathcal{P}_{10}^{({}^3S_1 \rightarrow {}^1S_0 + {}^1S_0)} = -\frac{2^5}{3^3} x, \tag{8}$$

$$\mathcal{P}_{20}^{({}^3P_2 \rightarrow {}^1S_0 + {}^1S_0)} = +\frac{2^6}{3^4 5^{1/2}} x^2, \tag{9}$$

$$\mathcal{P}_{21}^{({}^3P_2 \rightarrow {}^3S_1 + {}^1S_0)} = -\frac{2^{11/2}}{3^7 5^{1/2}} x^2, \tag{10}$$

$$\mathcal{P}_{01}^{({}^3P_1 \rightarrow {}^3S_1 + {}^1S_0)} = +\frac{2^5}{3^{5/2}} \left(1 - \frac{2}{9} x^2 \right), \tag{11}$$

$$\mathcal{P}_{21}^{({}^3P_1 \rightarrow {}^3S_1 + {}^1S_0)} = -\frac{2^{11/2}}{3^{9/2}} x^2, \tag{12}$$

$$\mathcal{P}_{00}^{({}^3P_0 \rightarrow {}^1S_0 + {}^1S_0)} = +\frac{2^{9/2}}{3^2} \left(1 - \frac{2}{9} x^2 \right), \tag{13}$$

$$\mathcal{P}_{01}^{({}^1P_1 \rightarrow {}^3S_1 + {}^1S_0)} = -\frac{2^{9/2}}{3^{5/2}} \left(1 - \frac{2}{9} x^2 \right), \tag{14}$$

$$\mathcal{P}_{21}^{({}^1P_1 \rightarrow {}^3S_1 + {}^1S_0)} = -\frac{2^6}{3^{9/2}} x^2. \tag{15}$$

For physical decays there is an additional multiplicative flavor factor, as discussed in Appendix A. In Fig. 1 we show these decay rates for physical mesons for a wide range of

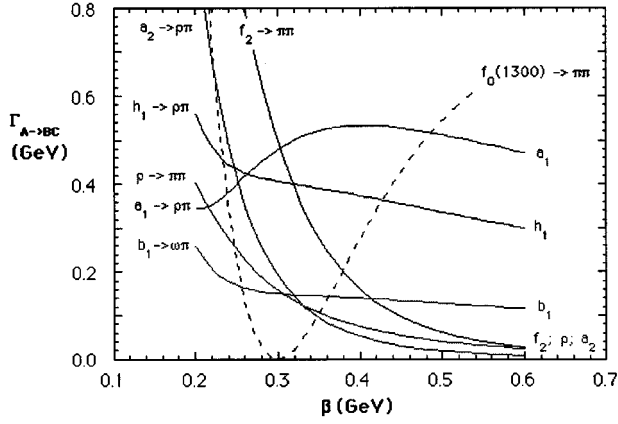


FIG. 1. Representative light $q\bar{q}$ meson decay rates in the 3P_0 decay model for $\gamma=0.5$.

wave function inverse length scales β . The scale β is defined in Appendix A; its numerical value is discussed below.

We set $\gamma=0.5$ in the figure because this is near the optimum fitted value. A value of $\beta \approx 0.35\text{--}0.4$ GeV evidently gives a reasonably accurate description of the relative decay rates (see also Table I below). Many recent quark model studies of meson [3–6] and baryon [10] decays use a value of $\beta=0.4$ GeV, at the upper end of this range.

A simple estimate of the optimum β for these SHO wave functions follows if we require maximum overlap with Coulomb plus linear wave functions Ψ . With typical quark model parameters of $\alpha_s=0.6$, $b=0.18$ GeV², and $m_q=0.33$ GeV, the overlap $|\int \Psi^* \psi_{\text{SHO}} d^3x|^2$ is maximum at $\beta=0.316$ GeV for $L_{q\bar{q}}=0$ (99.4% overlap) and $\beta=0.274$ GeV for $L_{q\bar{q}}=1$ (99.6% overlap). Curiously, this β would imply a narrow $f_0(1300)$ in the 3P_0 decay model. Comparison with Fig. 2 shows that these β estimates are similar to the values required to describe decays, although there is some evidence of a systematic discrepancy, $\beta_{\text{decay}}/\beta_{\text{Cou+lin}} \approx 1.2$.

In Table I we show a fit to a representative set of seven well-established light S - and P -wave $q\bar{q}$ meson decay rates, with β and γ taken as free parameters. The masses assumed were $M_\pi=0.138$ GeV, $M_K=0.496$ GeV, $M_\rho=0.77$ GeV, $M_\omega=0.782$ GeV, $M_{h_1}=1.17$ GeV, $M_{a_1}=1.23$ GeV, $M_{b_1}=1.231$ GeV, $M_{f_2}=1.275$ GeV, $M_{f_0}=1.3$ GeV, $M_{a_2}=1.318$ GeV, and $M_{K_0^*}=1.429$ GeV. All but $K_0^*(1430) \rightarrow K\pi$ are nonstrange systems, which we chose to

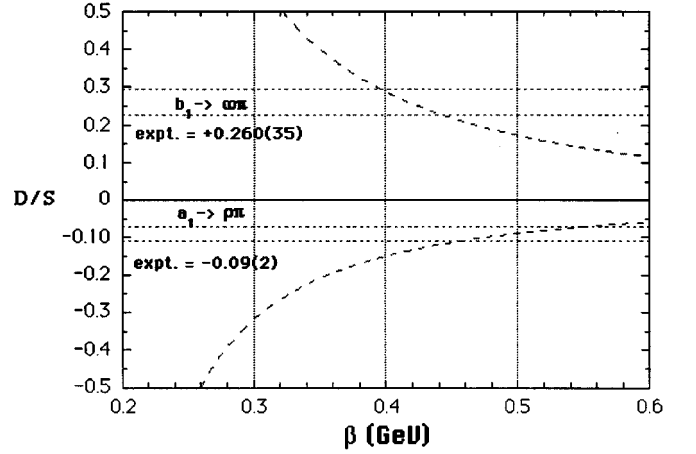


FIG. 2. D/S amplitude ratios in $b_1 \rightarrow \omega\pi$ and $a_1 \rightarrow \rho\pi$ with 3P_0 model predictions.

avoid parameter differences due to strange quarks. The $K_0^*(1430)$ is included because we found that it is quite important to include a light 3P_0 $q\bar{q}$ decay, since the rate ${}^3P_0 \rightarrow {}^1S_0 + {}^1S_0$ is quite sensitive to β , and the $K_0^*(1430)$ is the only well-established 3P_0 resonance. On fitting these widths using Eqs. (6)–(15) [minimizing $\sum_{i=1}^7 (\Gamma_{A \rightarrow BC}^{\text{thy}}/\Gamma_{A \rightarrow BC}^{\text{expt}} - 1)^2$], we find the parameters

$$\beta = 0.397 \text{ GeV}, \quad (16)$$

$$\gamma = 0.506. \quad (17)$$

Clearly, the most important discrepancy in the table is $\rho \rightarrow \pi\pi$, which is well known to be a problem relative to the decays of P -wave $q\bar{q}$ mesons in this model. The $K_0^*(1430)$ width is also rather smaller than experiment.

We stress that one cannot expect the fitted value of β to agree closely with the simple theoretical estimate given earlier. Different observables probe different regions of the meson wave functions, and since SHO wave functions are only approximate, different optimal values of β will arise from them. In view of this, it is natural to question the use of SHO wave functions. Experience indicates, however, that it is not useful to employ more accurate Coulomb plus linear wave functions in what must be highly simplified models of com-

TABLE I. A fit of the 3P_0 model to light meson decay rates ($\gamma=0.506$, $\beta=0.397$ GeV).

Decay	Expt. [11] MeV	3P_0 Theory MeV	D/S Expt. [11,12]	D/S 3P_0 Theory
$\rho \rightarrow \pi\pi$	151	79		
$f_2 \rightarrow \pi\pi$	157	170		
$a_2 \rightarrow \rho\pi$	72	54		
$a_1 \rightarrow \rho\pi$	400	545	-0.09(2)	-0.154
$b_1 \rightarrow \omega\pi$	142	143	+0.260(35)	+0.292
$h_1 \rightarrow \rho\pi$	360	383	–	+0.222
$K_0^*(1430) \rightarrow K\pi$	287	166		
$f_0 \rightarrow \pi\pi$	150–400 (not fitted)	271		

plex hadronic interactions (see, for example Refs. [4] and [5]). We therefore adopt the utilitarian approach of employing SHO wave functions, which lead to analytic decay rates, with β fixed at the optimal value of 0.4 GeV.

If we attempt constrained fits to γ with fixed β , we find serious disagreement with experiment for even moderate changes away from $\beta=0.4$ GeV. For example, at $\beta=0.3$ GeV we find an f_2 broader than the a_1 and h_1 , and a $K_0^*(1430)$ width near zero. Conversely, if we increase β to 0.5 GeV, we find quite small partial widths for $\rho \rightarrow \pi\pi$, $a_2 \rightarrow \rho\pi$, and $f_2 \rightarrow \pi\pi$ relative to the b_1 , a_1 , and h_1 , on average only 0.31 of $b_1 \rightarrow \omega\pi$; experimentally, the ratio is 0.89.

The interesting question of the width of an $f_0(1300) q\bar{q}$ state is unfortunately problematical in the 3P_0 model, since like $K_0^*(1430) \rightarrow K\pi$ this rate has a node near $\beta=0.30$ GeV, and increases rapidly with β above the node. With our fitted parameters we find $\Gamma_{f_0(1300) \rightarrow \pi\pi} = 271$ MeV, but comparison of the predicted and observed $K_0^*(1430)$ widths suggests that the actual $f_0(1300)$ partial width to $\pi\pi$ is ≈ 450 MeV. We shall show subsequently that the transition ${}^3P_0 \rightarrow {}^1S_0 + {}^1S_0$ has an the additional complication of an unusually large OGE decay amplitude, which may explain why the light scalars $f_0(1300)$ and $K_0^*(1430)$ are broad states despite the node in the 3P_0 decay amplitude.

B. 3P_0 results for D/S ratios

Sensitive tests of decay models are possible in decays with more than one partial wave because one can then measure the relative phases as well as the magnitudes of the decay amplitudes. Furthermore, these quantities are of theoretical interest because scale and phase space ambiguities cancel in the ratio.

Multiamplitude decays require at least one final meson to have nonzero spin. For the decays considered here, the relevant final states are $\rho\pi$ and $\omega\pi$; other possibilities are excluded by phase space. These final states have $S^P = 1^+$, so of all the light $L_{q\bar{q}}=0$ and $L_{q\bar{q}}=1$ mesons only the 1^+ mesons have more than one partial wave; these decay to both S - and D -wave vector-plus-pseudoscalar final states. On increasing $L_{q\bar{q}}$ we next encounter multiamplitude decays in the D states, for example in $\pi_2 \rightarrow \rho\pi$ (P, F) [4] and $\pi_2 \rightarrow f_2\pi$ (S, D, G).

Here we will calculate the D/S amplitude ratios for the decays $b_1 \rightarrow \omega\pi$ and $a_1 \rightarrow \rho\pi$. The ratio for $h_1 \rightarrow \rho\pi$, which has not been measured, is theoretically equal to $b_1 \rightarrow \omega\pi$ to within small phase space differences, since these are both ${}^1P_1 \rightarrow {}^3S_1 + {}^1S_0$ decays. The b_1 is clearly the most attractive of these experimentally, due to the smaller widths of the b_1 and ω .

We assume an initial polarization $b_1^+(J_z = +1)$ and determine the h_{fi} matrix element to a final state with a specific ω polarization that allows both L values; we choose $\omega(S_z = +1)$. Using the diagrammatic techniques of Appendix A, we find that the two diagrams d_1 and d_2 give equal contributions, and the total h_{fi} is

$$h_{fi} \Big|_{b_1^+ (+\hat{z}) \rightarrow \omega (+\hat{z}) \pi^+} = -\frac{\gamma}{\pi^{1/4} \beta^{1/2}} \frac{2^4}{3^{5/2}} \left[\left(1 - \frac{2}{9} x^2 \right) Y_{00}(\Omega) + \frac{2}{3^2 5^{1/2}} x^2 Y_{20}(\Omega) \right] e^{-x^2/12}. \quad (18)$$

This matrix element determines the relative S and D amplitudes in the $|\omega\pi\rangle$ final state; since the $J^P = 1^+ |\omega\pi\rangle$ state is of the form

$$|\omega\pi\rangle = a_S |{}^3S_1\rangle + a_D |{}^3D_1\rangle, \quad (19)$$

it follows from a Clebsch-Gordon decomposition that the amplitude to find a $(+\hat{z})$ -polarized ω in an $\omega\pi$ pair with recoil direction Ω must be

$$\langle \omega (+\hat{z})_{\Omega} \pi_{-\Omega} | \omega\pi \rangle = a_S Y_{00}(\Omega) + a_D \sqrt{\frac{1}{10}} Y_{20}(\Omega). \quad (20)$$

We can therefore read the a_D/a_S ratio directly from the h_{fi} matrix element (18),

$$\frac{a_D}{a_S} \Big|_{b_1 \rightarrow \omega\pi} = +\frac{2^{3/2}}{3^2} \frac{x^2}{\left(1 - \frac{2}{9} x^2 \right)}. \quad (21)$$

This is equivalent to the result (4.11,12) of Le Yaouanc *et al.* in the first reference of [2] when one specializes their result to equal wave function widths. This D/S ratio is also implicit in Eqs. (14) and (15). Since the strength of the pair production amplitude and some of the momentum dependence in the overlap integrals cancel out in this ratio, there is less systematic uncertainty than in the decay rates. Proceeding similarly for $a_1 \rightarrow \rho\pi$, we find

$$\frac{a_D}{a_S} \Big|_{a_1 \rightarrow \rho\pi} = -\frac{2^{1/2}}{3^2} \frac{x^2}{\left(1 - \frac{2}{9} x^2 \right)}. \quad (22)$$

The *ratio* of D/S ratios in these decays is especially interesting in the 3P_0 model because all the dependence on the spatial wave functions cancels. One finds

$$\frac{\frac{a_D}{a_S} \Big|_{a_1 \rightarrow \rho\pi}}{\frac{a_D}{a_S} \Big|_{b_1 \rightarrow \omega\pi}} = -\frac{1}{2}. \quad (23)$$

Experimentally these ratios are

$$\frac{a_D}{a_S} \Big|_{b_1 \rightarrow \omega\pi} = +0.260 \pm 0.035 \quad (24)$$

and from a recent ARGUS measurement [12]

$$\left. \frac{a_D}{a_S} \right|_{a_1 \rightarrow \rho \pi} = -0.09 \pm 0.02, \quad (25)$$

so the ratio is

$$\frac{\left. \frac{a_D}{a_S} \right|_{a_1 \rightarrow \rho \pi}}{\left. \frac{a_D}{a_S} \right|_{b_1 \rightarrow \omega \pi}} = -0.35 \pm 0.09. \quad (26)$$

Theory and experiment for these D/S ratios are compared in Fig. 2; a best fit to these D/S ratios alone gives $\beta = 0.448$ GeV, for which $(D/S)_{b_1 \rightarrow \omega \pi} = +0.219$ and $(D/S)_{a_1 \rightarrow \rho \pi} = -0.115$. (The small theoretical departure of the ratio from $-1/2$ is due to phase space differences.)

The experimental ratio (26) is approximately consistent with the 3P_0 prediction, but shows the need for a more accurate experimental determination, especially in $a_1 \rightarrow \rho \pi$. An improved D/S ratio measurement would allow an interesting test of the 3P_0 model, since the OGE decay mechanism predicts a departure of the ratio (23) from $-1/2$; we will discuss this in the next section.

In summary, the decay rates of light $L_{q\bar{q}}=0$ and $L_{q\bar{q}}=1$ mesons (Fig. 1) support $\beta \approx 0.40$ GeV, whereas the D/S amplitude ratios in $b_1 \rightarrow \omega \pi$ and $a_1 \rightarrow \rho \pi$ (Fig. 2) suggest a larger value, $\beta \approx 0.45$ GeV. These are both significantly larger than the $\beta \approx 0.3$ GeV which gives the maximum overlap with Coulomb plus linear wave functions. The situation is not improved dramatically by employing more accurate Coulomb plus linear wave functions, which indicates that the assumed decay interaction only approximates the actual mechanism.

III. ‘‘MICROSCOPIC’’ DECAY MODELS

A. Candidate pair production Hamiltonians

In microscopic decay models, one attempts to describe hadron strong decays in terms of quark and gluon degrees of freedom. The quark-gluon decay mechanism should give similar predictions to the reasonably accurate 3P_0 model, and should determine the strength γ of the 3P_0 interaction in terms of fundamental QCD parameters. There has been little previous work in this area. One exception is the study of open charm decays of $c\bar{c}$ resonances by Eichten *et al.* [13], who assumed that decays are due to pair production from the confining interaction. We will confirm this assumption for light quarkonia in most but not all cases. Eichten *et al.*, however, assumed that confinement is a Lorentz *vector* interaction; this is now believed to be incorrect. The currently accepted scalar form leads to quite different matrix elements.

We begin by assuming that strong decays are driven by the same interquark Hamiltonian which determines the spectrum, and that it incorporates scalar confinement and one gluon exchange. These interactions and their associated decay amplitudes are undoubtedly all present and should be added coherently. We will determine decay rates for the two-body decays discussed in the previous section, assuming the

appropriate field-theoretic generalization of the usual interquark Hamiltonian.

The current-current interactions due to the scalar confining interaction and one gluon exchange (OGE) can be written in the generic form

$$H_I = \frac{1}{2} \iint d^3x d^3y J^a(\vec{x}) K(|\vec{x}-\vec{y}|) J^a(\vec{y}). \quad (27)$$

The current J^a in Eq. (27) is assumed to be a color octet. The currents J (with the color dependence $\lambda^a/2$ factored out) and the kernels $K(r)$ for the interactions are

$$J = \begin{cases} \bar{\psi}\psi & \text{scalar confining interaction,} \\ \psi^\dagger\psi & \text{color Coulomb OGE,} \\ (\bar{\psi}\vec{\gamma}\psi)_T & \text{transverse OGE,} \end{cases} \quad (28)$$

$$K = \begin{cases} +\frac{3}{4}(br+S_0) & \text{scalar confining interaction,} \\ +\alpha_s/r & \text{color Coulomb OGE,} \\ -\alpha_s/r & \text{transverse OGE.} \end{cases} \quad (29)$$

The scalar confinement kernel is normalized so that $br+S_0$ is the static scalar potential of a color-singlet $q\bar{q}$ pair.

We refer to this general type of interaction as a JKJ decay model, and to the specific cases considered here as sKs , j^0Kj^0 , and j^TKj^T interactions. The decay Hamiltonian assumed by Eichten *et al.* [13] in their Eq. (3.2) is a special case of our form (27) with a j^0Kj^0 interaction. The 3P_0 model is also a special case of Eq. (27), with only a constant scalar term, $S_0 = (3^{5/2}/2^4)m_q\gamma$.

B. $JKJ A \rightarrow BC$ matrix elements: General results

An $A \rightarrow BC$ decay matrix element of the JKJ Hamiltonian (27) involves a pair-production current matrix element $\langle q\bar{q}|J|0\rangle$ times a scattering matrix element $\langle q_f|J|q_i\rangle$. Diagrammatically this corresponds to an interaction between an initial line and the produced pair, and there are four such diagrams (see Fig. 3). We label these using the 3P_0 -model quark line diagram labels d_1 and d_2 , with an additional q or \bar{q} subscript denoting which initial line the produced pair interacts with.

We specialize to the diagram d_{1q} for illustration. As in the 3P_0 model (see Appendix A) there is a Fermi ‘‘signature’’ phase, a flavor factor, and a spin+space overlap integral,

$$\langle BC|H_I|A\rangle_{d_{1q}} = I_{\text{signature}} I_{\text{color}} I_{\text{flavor}} \mathbf{I}_{\text{spin+space}}, \quad (30)$$

where

$$\mathbf{I}_{\text{spin+space}} = I_{\text{spin+space}} \delta(\vec{A} - \vec{B} - \vec{C}). \quad (31)$$

The Fermi signature arises due to ordering of the quark and antiquark operators. It may be read off from the diagram as the number of line crossings; in this case

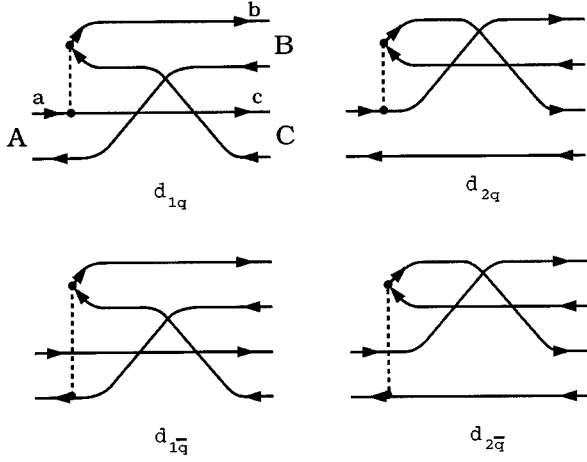


FIG. 3. The four independent $q\bar{q}$ meson decay diagrams in $J\bar{K}J$ decay models.

$I_{\text{signature}} = (-1)^3$. A new feature, due to our explicit treatment of color, is a color matrix element; the color factor for this diagram is

$$I_{\text{color}} = \frac{1}{3^{3/2}} \text{Tr} \left\{ \frac{\lambda^a}{2} \frac{\lambda^a}{2} \right\} = + \frac{2^2}{3^{3/2}} \quad (32)$$

and is the same for diagram d_{2q} and opposite for $d_{1\bar{q}}$ and $d_{2\bar{q}}$. The flavor and spin factors are specific to the reaction and will be discussed subsequently. The d_{1q} spatial overlap integral analogous to Eq. (A5) is

$$\begin{aligned} I_{\text{space}}(d_{1q}) &= 2! \iint d^3x d^3y \frac{1}{2} K(|\vec{x} - \vec{y}|) \\ &\times \iiint d^3a d^3b d^3c \phi_A(2\vec{a} - \vec{A}) \\ &\times \phi_B^*(2\vec{b} - \vec{B}) \phi_C^*(2\vec{c} - \vec{C}) \delta(\vec{A} - \vec{a} - \vec{B} + \vec{b}) \\ &\times \langle c | J(\vec{x}) | a \rangle \langle b\bar{c} | J(\vec{y}) | 0 \rangle, \end{aligned} \quad (33)$$

where the matrix elements of the currents (with $\Gamma = \gamma^0, \gamma^i, \mathbf{1}$) are

$$\langle q' | J(\vec{x}) | q \rangle = + \frac{1}{(2\pi)^3} \frac{m_q}{\sqrt{E_q E_{q'}}} e^{i(q' - q) \cdot x} [\bar{u}_{q's'} \Gamma u_{qs}], \quad (34)$$

$$\langle \bar{q}' | J(\vec{x}) | \bar{q} \rangle = - \frac{1}{(2\pi)^3} \frac{m_q}{\sqrt{E_q E_{q'}}} e^{i(\bar{q}' - \bar{q}) \cdot x} [\bar{v}_{\bar{q}'\bar{s}'} \Gamma v_{\bar{q}\bar{s}}], \quad (35)$$

and

$$\langle q\bar{q} | J(\vec{y}) | 0 \rangle = \frac{1}{(2\pi)^3} \frac{m_q}{\sqrt{E_q E_{\bar{q}}}} e^{i(q + \bar{q}) \cdot y} [\bar{u}_{qs} \Gamma v_{\bar{q}\bar{s}}]. \quad (36)$$

With these substitutions, and introducing a Fourier transformed kernel

$$\mathcal{K}(Q) = \int d^3x e^{i\vec{Q} \cdot \vec{r}} K(r) \quad (37)$$

we find

$$\begin{aligned} I_{\text{space}}(d_{1q}) &= \frac{1}{(2\pi)^3} \iint d^3a d^3c \phi_A(2\vec{a} - \vec{A}) \\ &\times \phi_B^*(2\vec{a} - 2\vec{C} - \vec{B}) \phi_C^*(2\vec{c} - \vec{C}) \frac{m_q^2}{\sqrt{E_a E_b E_c E_{\bar{c}}}} \\ &\times [\bar{u}_{bs_b} \Gamma v_{\bar{c}s_{\bar{c}}}] \mathcal{K}(|\vec{a} - \vec{c}|) [\bar{u}_{cs_c} \Gamma u_{as_a}] \end{aligned} \quad (38)$$

and there are implicit momentum constraints $\vec{b} = \vec{a} - \vec{C}$ and $\vec{c} = \vec{C} - \vec{c}$ from the spatial integrations in Eq. (33) and the meson wave functions.

As in the 3P_0 model, we take the nonrelativistic limit of this interaction for our decay amplitude, although it would be interesting in future work to investigate the effect of keeping the full relativistic amplitude (38). We also specialize to the rest frame, $\vec{A} = 0$ and $\vec{B} = -\vec{C}$. These substitutions give our final general result for the d_{1q} overlap integral,

$$\begin{aligned} I_{\text{space}}(d_{1q}) &= \frac{1}{(2\pi)^3} \iint d^3a d^3c \phi_A(2\vec{a}) \\ &\times \phi_B^*(2\vec{a} + \vec{B}) \phi_C^*(2\vec{c} + \vec{B}) \\ &\times [\bar{u}_{bs_b} \Gamma v_{\bar{c}s_{\bar{c}}}] \mathcal{K}(|\vec{a} - \vec{c}|) [\bar{u}_{cs_c} \Gamma u_{as_a}]. \end{aligned} \quad (39)$$

The overlap integrals associated with the three remaining diagrams are given in Appendix B, and the detailed evaluation of a decay amplitude \mathcal{M}_{LS} and a decay rate is illustrated in Appendix C for the decay $\rho \rightarrow \pi\pi$ with a $j^0 K j^0$ interaction.

C. $J\bar{K}J$ $A \rightarrow BC$ matrix elements: Explicit results for SHO wave functions

The complete decay amplitudes for the channels spanned by our representative set of light two-body meson decays are given below. The five expressions present in each $\tilde{\mathcal{M}}$ amplitude correspond to contributions from (1) the scalar confinement term, (2) the constant scalar term, (3) Coulomb OGE, (4) the portion of the transverse OGE operator which is proportional to δ_{ij} , and (5) the term in transverse OGE which is proportional to $-Q_i Q_j / \vec{Q}^2$. A common factor has been removed

$$\mathcal{M}_{LS} = \frac{\beta^{1/2}}{\pi^{3/4} m_q} e^{-x^2/12} \tilde{\mathcal{M}}_{LS}. \quad (40)$$

The results for each channel are

$$\begin{aligned}
\mathcal{M}_{10}^{(3S_1 \rightarrow 1S_0 + 1S_0)} = & -\frac{2^3 5}{3^3} \left(\frac{b}{\beta^2} \right) x \left[{}_1F_1 \left(-\frac{1}{2}; \frac{3}{2}; \xi \right) + \frac{4}{45} {}_1F_1 \left(-\frac{1}{2}; \frac{5}{2}; \xi \right) \right] - \frac{2^9}{3^{11/2}} \pi^{1/2} \left(\frac{S_0}{\beta} \right) x + \frac{2^3}{3^3} \alpha_s x \left[{}_1F_1 \left(\frac{1}{2}; \frac{3}{2}; \xi \right) \right. \\
& \left. - \frac{2}{3} {}_1F_1 \left(\frac{1}{2}; \frac{5}{2}; \xi \right) \right] + \frac{2^3}{3^3} \alpha_s x \left[{}_1F_1 \left(\frac{1}{2}; \frac{3}{2}; \xi \right) + \frac{10}{9} {}_1F_1 \left(\frac{1}{2}; \frac{5}{2}; \xi \right) \right] - \frac{2^3}{3^2} \alpha_s x \left[{}_1F_1 \left(\frac{1}{2}; \frac{3}{2}; \xi \right) - \frac{2}{3} {}_1F_1 \left(\frac{1}{2}; \frac{5}{2}; \xi \right) \right], \tag{41}
\end{aligned}$$

$$\begin{aligned}
\mathcal{M}_{20}^{(3P_2 \rightarrow 1S_0 + 1S_0)} = & + \frac{2^2 5^{1/2}}{3^3} \left(\frac{b}{\beta^2} \right) x^2 \left[{}_1F_1 \left(-\frac{1}{2}; \frac{3}{2}; \xi \right) + \frac{8}{15} {}_1F_1 \left(-\frac{1}{2}; \frac{5}{2}; \xi \right) + \frac{8}{225} {}_1F_1 \left(-\frac{1}{2}; \frac{7}{2}; \xi \right) \right] \\
& + \frac{2^{10}}{3^{13/2} 5^{1/2}} \pi^{1/2} \left(\frac{S_0}{\beta} \right) x^2 - \frac{2^2}{3^3 5^{1/2}} \alpha_s x^2 \left[{}_1F_1 \left(\frac{1}{2}; \frac{3}{2}; \xi \right) - \frac{4}{9} {}_1F_1 \left(\frac{1}{2}; \frac{5}{2}; \xi \right) - \frac{8}{45} {}_1F_1 \left(\frac{1}{2}; \frac{7}{2}; \xi \right) \right] \\
& - \frac{2^2}{3^3 5^{1/2}} \alpha_s x^2 \left[{}_1F_1 \left(\frac{1}{2}; \frac{3}{2}; \xi \right) + \frac{4}{3} {}_1F_1 \left(\frac{1}{2}; \frac{5}{2}; \xi \right) + \frac{8}{27} {}_1F_1 \left(\frac{1}{2}; \frac{7}{2}; \xi \right) \right] + \frac{2^2}{3^2 5^{1/2}} \alpha_s x^2 \left[{}_1F_1 \left(\frac{1}{2}; \frac{3}{2}; \xi \right) \right. \\
& \left. - \frac{8}{27} {}_1F_1 \left(\frac{1}{2}; \frac{5}{2}; \xi \right) - \frac{8}{27} {}_1F_1 \left(\frac{1}{2}; \frac{7}{2}; \xi \right) \right], \tag{42}
\end{aligned}$$

$$\begin{aligned}
\mathcal{M}_{21}^{(3P_2 \rightarrow 3S_1 + 1S_0)} = & -\frac{2^{3/2} 5^{1/2}}{3^{5/2}} \left(\frac{b}{\beta^2} \right) x^2 \left[{}_1F_1 \left(-\frac{1}{2}; \frac{3}{2}; \xi \right) + \frac{8}{15} {}_1F_1 \left(-\frac{1}{2}; \frac{5}{2}; \xi \right) + \frac{8}{225} {}_1F_1 \left(-\frac{1}{2}; \frac{7}{2}; \xi \right) \right] - \frac{2^{19/2}}{3^6 5^{1/2}} \pi^{1/2} \left(\frac{S_0}{\beta} \right) x^2 \\
& + \frac{2^{3/2}}{3^{5/2} 5^{1/2}} \alpha_s x^2 \left[{}_1F_1 \left(\frac{1}{2}; \frac{3}{2}; \xi \right) - \frac{4}{9} {}_1F_1 \left(\frac{1}{2}; \frac{5}{2}; \xi \right) - \frac{8}{45} {}_1F_1 \left(\frac{1}{2}; \frac{7}{2}; \xi \right) \right] + \frac{2^{5/2}}{3^{5/2} 5^{1/2}} \alpha_s x^2 \left[{}_1F_1 \left(\frac{1}{2}; \frac{3}{2}; \xi \right) \right. \\
& \left. + \frac{4}{9} {}_1F_1 \left(\frac{1}{2}; \frac{5}{2}; \xi \right) + \frac{8}{135} {}_1F_1 \left(\frac{1}{2}; \frac{7}{2}; \xi \right) \right] - \frac{2^{3/2}}{3^3 5^{1/2}} \alpha_s x^2 \left[{}_1F_1 \left(\frac{1}{2}; \frac{3}{2}; \xi \right) - \frac{8}{27} {}_1F_1 \left(\frac{1}{2}; \frac{5}{2}; \xi \right) - \frac{8}{27} {}_1F_1 \left(\frac{1}{2}; \frac{7}{2}; \xi \right) \right], \tag{43}
\end{aligned}$$

$$\begin{aligned}
\mathcal{M}_{01}^{(3P_1 \rightarrow 3S_1 + 1S_0)} = & -\frac{2^5 5}{3^{7/2}} \left(\frac{b}{\beta^2} \right) \left[{}_1F_1 \left(-\frac{3}{2}; -\frac{1}{2}; \xi \right) - \frac{12}{5} {}_1F_1 \left(-\frac{3}{2}; \frac{1}{2}; \xi \right) + \frac{8}{15} {}_1F_1 \left(-\frac{3}{2}; \frac{3}{2}; \xi \right) \right] + \frac{2^9}{3^5} \pi^{1/2} \left(\frac{S_0}{\beta} \right) \left(1 - \frac{2}{9} x^2 \right) \\
& + \frac{2^5}{3^{5/2}} \alpha_s \left[{}_1F_1 \left(-\frac{1}{2}; -\frac{1}{2}; \xi \right) + \frac{4}{3} {}_1F_1 \left(-\frac{1}{2}; \frac{1}{2}; \xi \right) - \frac{8}{3} {}_1F_1 \left(-\frac{1}{2}; \frac{3}{2}; \xi \right) \right] + \frac{2^6}{3^{5/2}} \alpha_s \left[{}_1F_1 \left(-\frac{1}{2}; -\frac{1}{2}; \xi \right) \right. \\
& \left. - \frac{10}{3} {}_1F_1 \left(-\frac{1}{2}; \frac{1}{2}; \xi \right) + \frac{28}{9} {}_1F_1 \left(-\frac{1}{2}; \frac{3}{2}; \xi \right) \right] - \frac{2^5}{3^{3/2}} \alpha_s \left[{}_1F_1 \left(-\frac{1}{2}; -\frac{1}{2}; \xi \right) \right. \\
& \left. + \frac{8}{9} {}_1F_1 \left(-\frac{1}{2}; \frac{1}{2}; \xi \right) - \frac{16}{9} {}_1F_1 \left(-\frac{1}{2}; \frac{3}{2}; \xi \right) \right], \tag{44}
\end{aligned}$$

$$\begin{aligned}
\mathcal{M}_{21}^{(3P_1 \rightarrow 3S_1 + 1S_0)} = & -\frac{2^{3/2} 5}{3^{7/2}} \left(\frac{b}{\beta^2} \right) x^2 \left[{}_1F_1 \left(-\frac{1}{2}; \frac{3}{2}; \xi \right) + \frac{8}{15} {}_1F_1 \left(-\frac{1}{2}; \frac{5}{2}; \xi \right) + \frac{8}{225} {}_1F_1 \left(-\frac{1}{2}; \frac{7}{2}; \xi \right) \right] - \frac{2^{19/2}}{3^7} \pi^{1/2} \left(\frac{S_0}{\beta} \right) x^2 \\
& + \frac{2^{3/2}}{3^{7/2}} \alpha_s x^2 \left[{}_1F_1 \left(\frac{1}{2}; \frac{3}{2}; \xi \right) - \frac{4}{9} {}_1F_1 \left(\frac{1}{2}; \frac{5}{2}; \xi \right) - \frac{8}{45} {}_1F_1 \left(\frac{1}{2}; \frac{7}{2}; \xi \right) \right] + \frac{2^{5/2}}{3^{7/2}} \alpha_s x^2 \left[{}_1F_1 \left(\frac{1}{2}; \frac{3}{2}; \xi \right) + \frac{4}{9} {}_1F_1 \left(\frac{1}{2}; \frac{5}{2}; \xi \right) \right. \\
& \left. + \frac{8}{135} {}_1F_1 \left(\frac{1}{2}; \frac{7}{2}; \xi \right) \right] - \frac{2^{3/2}}{3^{5/2}} \alpha_s x^2 \left[{}_1F_1 \left(\frac{1}{2}; \frac{3}{2}; \xi \right) - \frac{8}{27} {}_1F_1 \left(\frac{1}{2}; \frac{5}{2}; \xi \right) - \frac{8}{27} {}_1F_1 \left(\frac{1}{2}; \frac{7}{2}; \xi \right) \right], \tag{45}
\end{aligned}$$

$$\begin{aligned}
\mathcal{M}_{00}^{(3P_0 \rightarrow 1S_0 + 1S_0)} = & -\frac{2^{9/2}5}{3^3} \left(\frac{b}{\beta^2}\right) \left[{}_1F_1\left(-\frac{3}{2}; -\frac{1}{2}; \xi\right) - \frac{12}{5} {}_1F_1\left(-\frac{3}{2}; \frac{1}{2}; \xi\right) + \frac{8}{15} {}_1F_1\left(-\frac{3}{2}; \frac{3}{2}; \xi\right) \right] + \frac{2^{17/2}}{3^{9/2}} \pi^{1/2} \left(\frac{S_0}{\beta}\right) \left(1 - \frac{2}{9}x^2\right) \\
& + \frac{2^{9/2}}{3^2} \alpha_s \left[{}_1F_1\left(-\frac{1}{2}; -\frac{1}{2}; \xi\right) + \frac{4}{3} {}_1F_1\left(-\frac{1}{2}; \frac{1}{2}; \xi\right) - \frac{8}{3} {}_1F_1\left(-\frac{1}{2}; \frac{3}{2}; \xi\right) \right] + \frac{2^{9/2}}{3^2} \alpha_s \left[{}_1F_1\left(-\frac{1}{2}; -\frac{1}{2}; \xi\right) \right. \\
& - 8 {}_1F_1\left(-\frac{1}{2}; \frac{1}{2}; \xi\right) + \frac{80}{9} {}_1F_1\left(-\frac{1}{2}; \frac{3}{2}; \xi\right) \left. \right] - \frac{2^{9/2}}{3} \alpha_s \left[{}_1F_1\left(-\frac{1}{2}; -\frac{1}{2}; \xi\right) \right. \\
& \left. + \frac{8}{9} {}_1F_1\left(-\frac{1}{2}; \frac{1}{2}; \xi\right) - \frac{16}{9} {}_1F_1\left(-\frac{1}{2}; \frac{3}{2}; \xi\right) \right], \tag{46}
\end{aligned}$$

$$\begin{aligned}
\mathcal{M}_{01}^{(1P_1 \rightarrow 3S_1 + 1S_0)} = & + \frac{2^{9/2}5}{3^{7/2}} \left(\frac{b}{\beta^2}\right) \left[{}_1F_1\left(-\frac{3}{2}; -\frac{1}{2}; \xi\right) - \frac{12}{5} {}_1F_1\left(-\frac{3}{2}; \frac{1}{2}; \xi\right) + \frac{8}{15} {}_1F_1\left(-\frac{3}{2}; \frac{3}{2}; \xi\right) \right] - \frac{2^{17/2}}{3^5} \pi^{1/2} \left(\frac{S_0}{\beta}\right) \left(1 - \frac{2}{9}x^2\right) \\
& - \frac{2^{9/2}}{3^{5/2}} \alpha_s \left[{}_1F_1\left(-\frac{1}{2}; -\frac{1}{2}; \xi\right) + \frac{4}{3} {}_1F_1\left(-\frac{1}{2}; \frac{1}{2}; \xi\right) - \frac{8}{3} {}_1F_1\left(-\frac{1}{2}; \frac{3}{2}; \xi\right) \right] - \frac{2^{9/2}}{3^{3/2}} \alpha_s \left[{}_1F_1\left(-\frac{1}{2}; -\frac{1}{2}; \xi\right) \right. \\
& - \frac{16}{9} {}_1F_1\left(-\frac{1}{2}; \frac{1}{2}; \xi\right) + \frac{32}{27} {}_1F_1\left(-\frac{1}{2}; \frac{3}{2}; \xi\right) \left. \right] + \frac{2^{9/2}}{3^{3/2}} \alpha_s \left[{}_1F_1\left(-\frac{1}{2}; -\frac{1}{2}; \xi\right) \right. \\
& \left. + \frac{8}{9} {}_1F_1\left(-\frac{1}{2}; \frac{1}{2}; \xi\right) - \frac{16}{9} {}_1F_1\left(-\frac{1}{2}; \frac{3}{2}; \xi\right) \right], \tag{47}
\end{aligned}$$

$$\begin{aligned}
\mathcal{M}_{21}^{(1P_1 \rightarrow 3S_1 + 1S_0)} = & -\frac{2^2 5}{3^{7/2}} \left(\frac{b}{\beta^2}\right) x^2 \left[{}_1F_1\left(-\frac{1}{2}; \frac{3}{2}; \xi\right) + \frac{8}{15} {}_1F_1\left(-\frac{1}{2}; \frac{5}{2}; \xi\right) + \frac{8}{225} {}_1F_1\left(-\frac{1}{2}; \frac{7}{2}; \xi\right) \right] - \frac{2^{10}}{3^7} \pi^{1/2} \left(\frac{S_0}{\beta}\right) x^2 \\
& + \frac{2^2}{3^{7/2}} \alpha_s x^2 \left[{}_1F_1\left(\frac{1}{2}; \frac{3}{2}; \xi\right) - \frac{4}{9} {}_1F_1\left(\frac{1}{2}; \frac{5}{2}; \xi\right) - \frac{8}{45} {}_1F_1\left(\frac{1}{2}; \frac{7}{2}; \xi\right) \right] + \frac{2^2}{3^{5/2}} \alpha_s x^2 \left[{}_1F_1\left(\frac{1}{2}; \frac{3}{2}; \xi\right) \right. \\
& \left. + \frac{4}{27} {}_1F_1\left(\frac{1}{2}; \frac{5}{2}; \xi\right) - \frac{8}{405} {}_1F_1\left(\frac{1}{2}; \frac{7}{2}; \xi\right) \right] - \frac{2^2}{3^{5/2}} \alpha_s x^2 \left[{}_1F_1\left(\frac{1}{2}; \frac{3}{2}; \xi\right) - \frac{8}{27} {}_1F_1\left(\frac{1}{2}; \frac{5}{2}; \xi\right) - \frac{8}{27} {}_1F_1\left(\frac{1}{2}; \frac{7}{2}; \xi\right) \right]. \tag{48}
\end{aligned}$$

D. JKJ decay rates: Numerical results

To estimate the numerical importance of the scalar and OGE decay mechanisms, we first specialize to $\rho \rightarrow \pi\pi$ and consider each contribution in isolation. Using Eqs. (6), (40), and (41), and the flavor factors in Appendix A, the decay rate due to linear scalar pair production alone would be

$$\begin{aligned}
\Gamma_{\rho \rightarrow \pi\pi}^{sKs} = & \pi^{-1/2} \left(\frac{2^6 5^2}{3^6}\right) \left(\frac{b}{m_q \beta}\right)^2 \frac{E_\pi^2}{M_\rho} x^3 \left[{}_1F_1\left(-\frac{1}{2}; \frac{3}{2}; \xi\right) \right. \\
& \left. + \frac{4}{45} {}_1F_1\left(-\frac{1}{2}; \frac{5}{2}; \xi\right) \right]^2 e^{-x^2/6}. \tag{49}
\end{aligned}$$

The analogous decay rates due to Coulomb OGE and transverse OGE are

$$\begin{aligned}
\Gamma_{\rho \rightarrow \pi\pi}^{j^0 K j^0} = & \pi^{-1/2} \left(\frac{2^6}{3^6}\right) \alpha_s^2 \left(\frac{\beta}{m_q}\right)^2 \frac{E_\pi^2}{M_\rho} x^3 \left[{}_1F_1\left(\frac{1}{2}; \frac{3}{2}; \xi\right) \right. \\
& \left. - \frac{2}{3} {}_1F_1\left(\frac{1}{2}; \frac{5}{2}; \xi\right) \right]^2 e^{-x^2/6} \tag{50}
\end{aligned}$$

and

$$\begin{aligned}
\Gamma_{\rho \rightarrow \pi\pi}^{j^T K j^T} = & \pi^{-1/2} \left(\frac{2^8}{3^6}\right) \alpha_s^2 \left(\frac{\beta}{m_q}\right)^2 \frac{E_\pi^2}{M_\rho} x^3 \left[{}_1F_1\left(\frac{1}{2}; \frac{3}{2}; \xi\right) \right. \\
& \left. + \frac{4}{9} {}_1F_1\left(\frac{1}{2}; \frac{5}{2}; \xi\right) \right]^2 e^{-x^2/6}. \tag{51}
\end{aligned}$$

These rates are shown in Fig. 4 for the parameter set $\alpha_s=0.6$, $b=0.18$ GeV², and $m_q=0.33$ GeV.

For comparison with the microscopic decay model amplitudes, we also show 3P_0 model decay amplitudes in Fig. 5; these assume $\gamma=0.5$, corresponding to $S_0=+0.161$ GeV. [Recall that the 3P_0 interaction is identical to a constant scalar term $S_0=(3^{5/2}/2^4)\gamma m_q$.]

Evidently, the dominant decay mechanism is the sKs interaction, pair production through the scalar confining potential. At $\beta=0.4$ GeV, the $\rho \rightarrow \pi\pi$ width predicted by the sKs model alone is 330 MeV, about twice the experimental 151 MeV. In comparison, transverse OGE gives a width of 3.9 MeV, and the color Coulomb interaction gives only 0.36

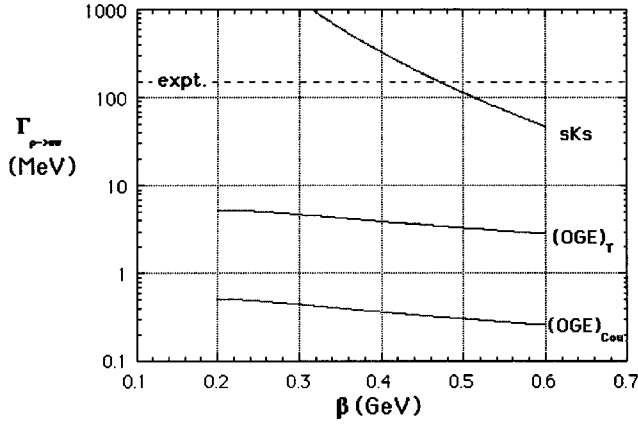


FIG. 4. The decay rate $\Gamma_{\rho \rightarrow \pi\pi}$ assuming only sKs , $j^T K j^T$ or $j^0 K j^0$ decay interactions. Parameters $\alpha_s=0.6$, $b=0.18 \text{ GeV}^2$, $m_q=0.33 \text{ GeV}$.

MeV. (The transverse and Coulomb OGE contributions add constructively, so the total width from OGE alone would be 6.7 MeV. These both interfere destructively with the dominant sKs amplitude, so the total width we find from all three amplitudes is $\Gamma_{\rho \rightarrow \pi\pi} = 243 \text{ MeV}$.)

Although the sKs interaction is usually found to be dominant in our representative set of decays, the OGE contribu-

tions are often comparable to sKs and cannot generally be ignored. To illustrate this, in Fig. 5 we show the numerical decay amplitudes we find for each decay. The normalization incorporates phase space, so these amplitudes squared give the physical decay rates. The magnitude of the experimental amplitude is indicated by horizontal lines. (The h_1 amplitudes are not shown because they are essentially identical to the b_1 amplitudes times a flavor factor of $\sqrt{3}$.)

The decay amplitudes due to Coulomb and transverse OGE also are shown in the histograms. The Coulomb gluon term is small in all the decays we have considered. This could have been anticipated; in the limit of a constant kernel K , the Coulomb gluon decay amplitude actually vanishes because the transition operator is then proportional to the fermion number operator $Q = \int d^3x j^0$ (squared), and hence cannot pair produce. With a slowly varying kernel the Coulomb decay amplitude is nonzero, but remains small. Transverse gluon exchange in contrast is sufficiently large to make an important contribution in some channels. The most notable of these are $K_0^* \rightarrow K\pi$ and $f_0 \rightarrow \pi\pi$, in which the OGE decay amplitude actually dominates the nonperturbative sKs amplitude [see Figs. 5(h) and 5(i)]. Recall that the widths of scalar $q\bar{q}$ states are problematical in the 3P_0 model because of a node in their decay amplitudes (see Fig. 1). The large additional OGE decay amplitude insures that the scalar

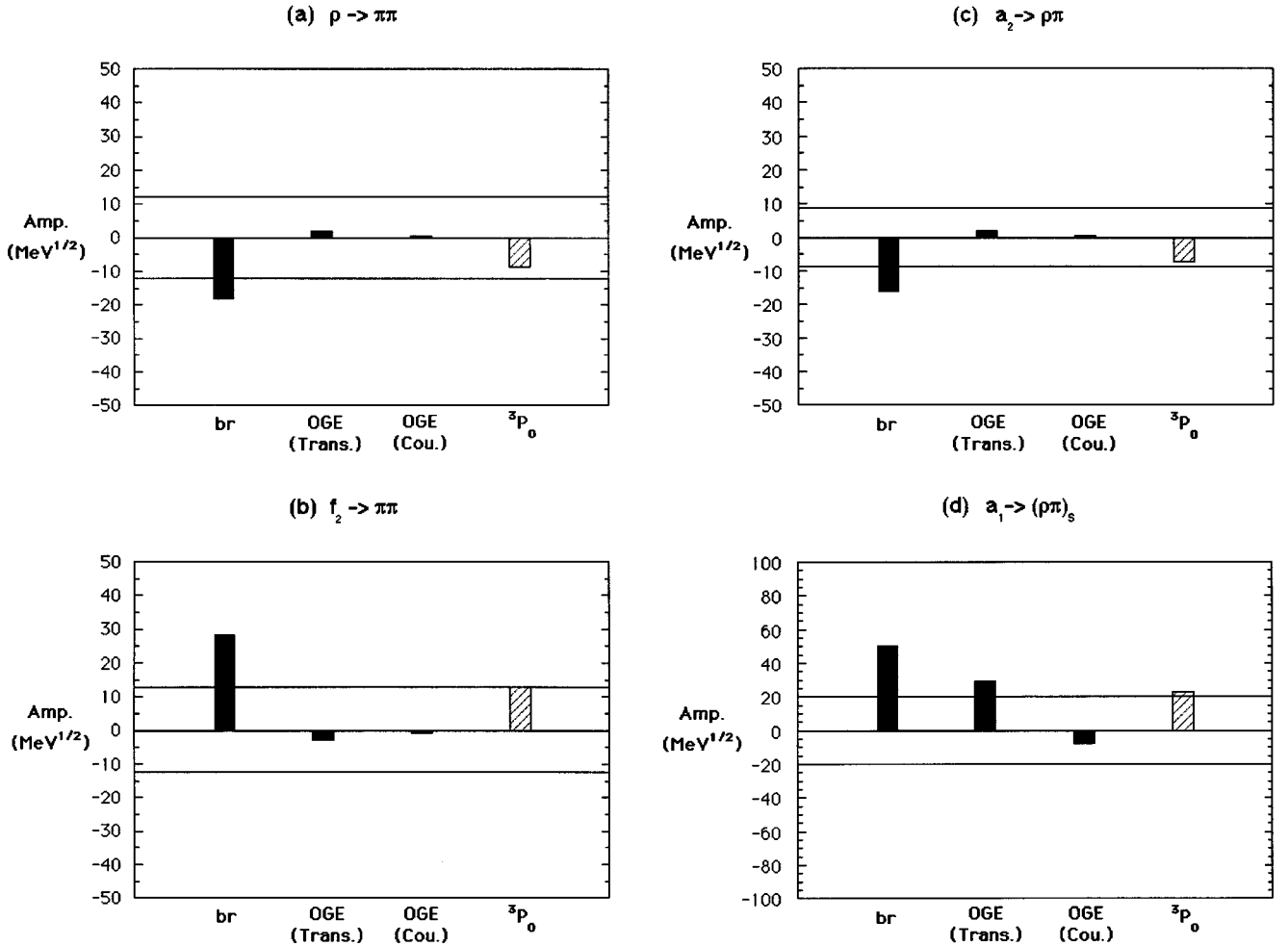


FIG. 5. (a)–(i) Decay amplitudes from sKs (br only), OGE (transverse), and OGE (Coulomb) decay mechanisms, with parameters $\beta=0.4 \text{ GeV}$, $b=0.18 \text{ GeV}^2$, $\alpha_s=0.6$, and $m_q=0.33 \text{ GeV}$. The decay amplitudes for the 3P_0 model of Sec. II are shown for comparison.

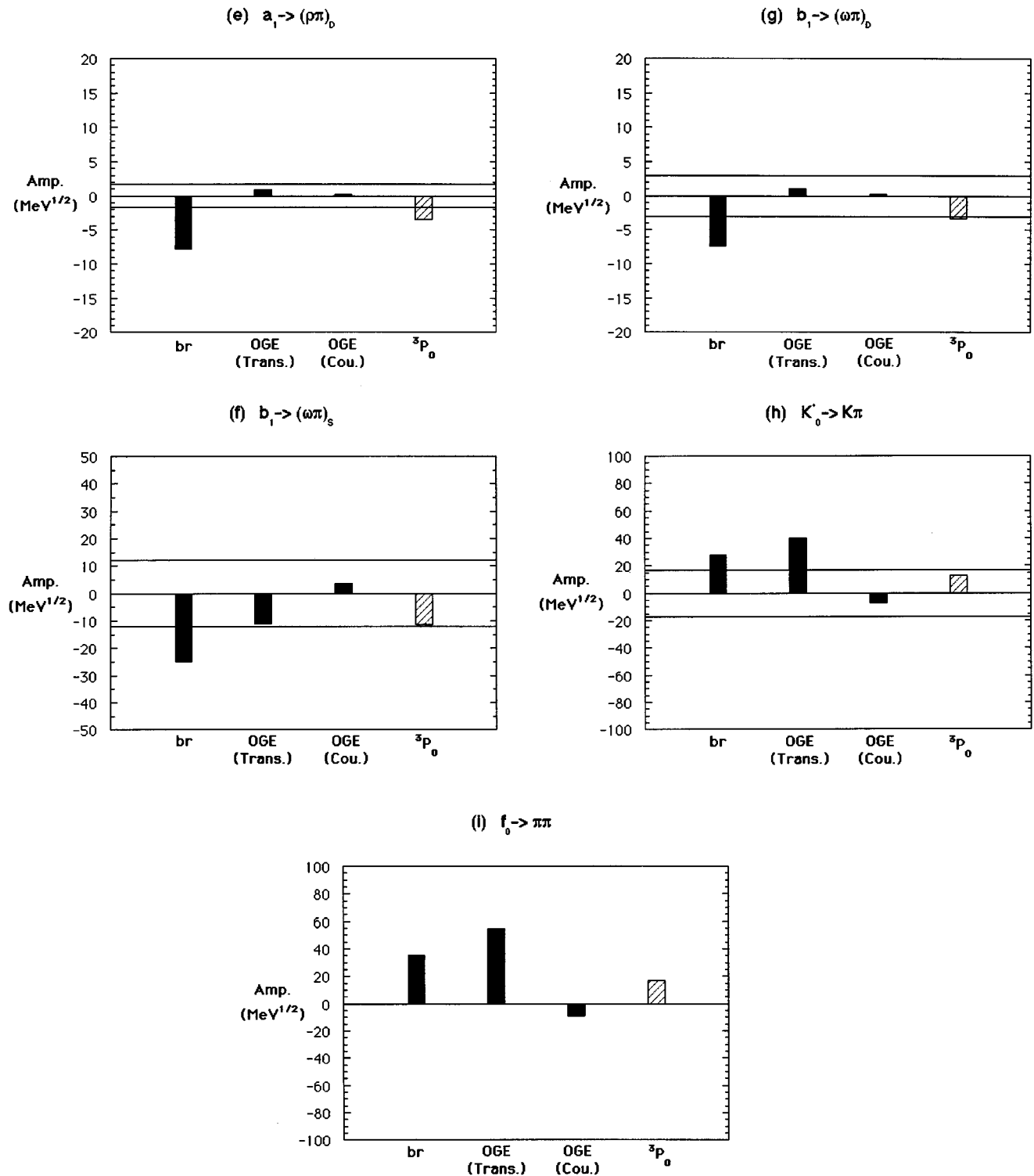


FIG. 5 (Continued).

$q\bar{q}$ states will be broad resonances, despite the node in the sKs or 3P_0 decay amplitudes.

Note that the overall scale of the total decay amplitudes predicted by the sKs +OGE decay mechanisms is too large relative to data by about a factor of two. It is nontrivial that there is even approximate agreement; recall in contrast that the overall scale of the decay rates is not determined in the 3P_0 model, but is fitted using the parameter γ . Since we regard the values $\alpha_s=0.6$, $b=0.18$ GeV², and $m_q=0.33$

GeV as reasonably well established for light quarks, we doubt that the discrepancy reflects our choices for these parameters. For this reason we do not show an optimized fit to the experimental rates, which would give reduced values for α_s and b .

We suggest that the theoretical overestimate of scale may be due to relativistic corrections to our nonrelativistic amplitudes, such as m/E factors in Eq. (38); if included, these would reduce the overall scale of rates and have little effect

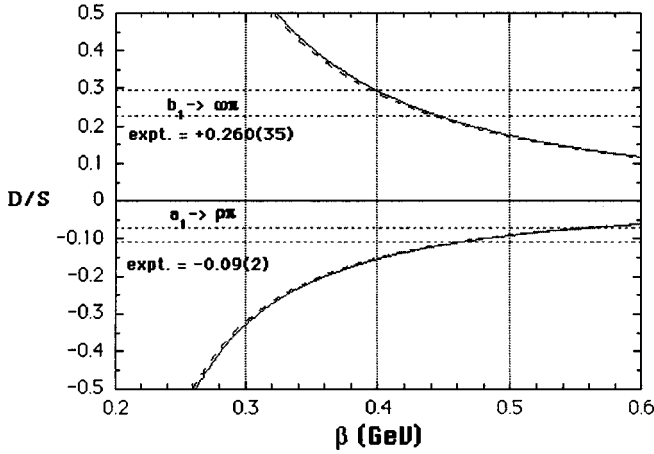


FIG. 6. D/S ratios in $b_1 \rightarrow \omega\pi$ and $a_1 \rightarrow \rho\pi$ predicted by the 3P_0 model (dashed) and the sKs model with $S(r)=br$ (solid).

on the successful relative rate predictions. Other possible sources of this discrepancy include our choice of $q\bar{q}$ wave functions (the overall scale of rates is sensitive to the SHO width parameter β) and our assumption that confinement may be treated as the exchange of a scalar quantum with a linear kernel in configuration space, but no q - q -scalar form factor.

A large negative constant S_0 of up to ≈ -1 GeV is often included in potential models, and is needed to give a best fit to spectroscopy. Of course, it may not actually be present in

the scalar potential $S(r)$, and may instead simply be a way of subtracting off a fictitious constituent quark mass contribution of $2m_q \approx 0.7$ GeV from the $q\bar{q}$ spectrum. If an S_0 of approximately this magnitude actually were present, it would make an important contribution, as it is larger than the br term and opposite in sign. We find however that an S_0 of this magnitude leads to unrealistic D/S ratios in $b_1 \rightarrow \omega\pi$ and $a_1 \rightarrow \rho\pi$. In both decays D/S passes through zero near $S_0 = -0.3$ GeV and diverges near $S_0 = -0.5$ GeV with conventional parameter values of $\alpha_s = 0.6$, $\beta = 0.4$ GeV, $b = 0.18$ GeV², and $m_q = 0.33$ GeV, whereas $S_0 = 0$ leads to reasonable D/S values. Since the D/S ratios are inconsistent with a large negative constant S_0 we will assume $S_0 = 0$ subsequently.

E. D/S ratios in JKJ decay models

In Sec. II B we noted that the ratio of S - and D -wave amplitudes in the decays $b_1 \rightarrow \omega\pi$ and $a_1 \rightarrow \rho\pi$ allowed sensitive tests of the angular quantum numbers of the $q\bar{q}$ pair produced in a strong decay, and that the 3P_0 model is in reasonable agreement with experiment, *albeit* for the rather large value of $\beta = 0.45$ GeV. Recall also that the ratio of D/S ratios (a_1/b_1) in the 3P_0 model is predicted to be $-1/2$ (neglecting minor phase space differences), independent of the $L_{q\bar{q}} = 0$ and $L_{q\bar{q}} = 1$ radial wave functions.

We find that the sKs interaction leads to very similar D/S predictions to the 3P_0 model. The sKs predictions for D/S ratios can be read from the decay amplitudes (41)–(48); for $b_1 \rightarrow \omega\pi$ it is

$$\frac{a_D}{a_S} \Big|_{b_1 \rightarrow \omega\pi}^{sKs} = -\frac{x^2 [{}_1F_1(-\frac{1}{2}; \frac{3}{2}; \xi) + \frac{8}{15} {}_1F_1(-\frac{1}{2}; \xi) + \frac{8}{225} {}_1F_1(-\frac{1}{2}; \frac{7}{2}; \xi)]}{2^{5/2} [{}_1F_1(-\frac{3}{2}; -\frac{1}{2}; \xi) - \frac{12}{5} {}_1F_1(-\frac{3}{2}; \frac{1}{2}; \xi) + \frac{8}{15} {}_1F_1(-\frac{3}{2}; \frac{3}{2}; \xi)]}. \quad (52)$$

This rather complicated result is shown as a function of β in Fig. 6, together with the 3P_0 prediction (21) and the corresponding $a_1 \rightarrow \rho\pi$ results. The sKs and 3P_0 decay models evidently give remarkably similar D/S ratios, and are essentially indistinguishable in these reactions.

The ratio of a_1/b_1 D/S ratios with the sKs interaction is predicted to be

$$\frac{\frac{a_D}{a_S} \Big|_{a_1 \rightarrow \rho\pi}}{\frac{a_D}{a_S} \Big|_{b_1 \rightarrow \omega\pi}} = -\frac{1}{2} \quad (53)$$

just as in the 3P_0 model. Thus, to the extent that the 3P_0 model is successful in explaining D/S ratios, this is a success of the sKs model as well. Some similarity could have been

anticipated since both decay models assume pair production with 3P_0 quantum numbers, and differ only in the presence or absence of spatial correlations with incoming quark lines.

The simple ratio in Eq. (53) follows in the $j^0 K j^0$ model as well, and appears to be generally true if the initial lines have no spin-flip amplitude and identical (a_1, b_1) and (ρ, ω, π) radial wave functions are assumed. In contrast, the $j^T K j^T$ transverse OGE interaction has an initial-line spin-flip amplitude, so the ratio departs from $-1/2$. This may be useful as a signature of the OGE component of the decay amplitude.

Although these D/S ratios are often cited as an argument against an OGE decay mechanism, the actual OGE calculation does not appear to have been carried out in the literature. (We emphasize that OGE is not equivalent to the “ 3S_1 ” decay model, for which results do exist [4,7].) We find that the full (Coulomb + transverse) OGE D/S ratios are given by

$$\frac{a_D}{a_S} \Big|_{b_1 \rightarrow \omega\pi}^{\text{OGE}} = - \frac{x^2 [{}_1F_1(\frac{1}{2}; \frac{3}{2}; \xi) + \frac{8}{9} {}_1F_1(\frac{1}{2}; \frac{5}{2}; \xi) + \frac{88}{135} {}_1F_1(\frac{1}{2}; \frac{7}{2}; \xi)]}{2^{5/2} 3 [{}_1F_1(-\frac{1}{2}; -\frac{1}{2}; \xi) - \frac{20}{3} {}_1F_1(-\frac{1}{2}; \frac{1}{2}; \xi) + \frac{56}{9} {}_1F_1(-\frac{1}{2}; \frac{3}{2}; \xi)]} \quad (54)$$

and

$$\frac{a_D}{a_S} \Big|_{a_1 \rightarrow \rho\pi}^{\text{OGE}} = - \frac{x^2 [{}_1F_1(\frac{1}{2}; \frac{5}{2}; \xi) + \frac{28}{45} {}_1F_1(\frac{1}{2}; \frac{7}{2}; \xi)]}{2^{9/2} 3^2 [{}_1F_1(-\frac{1}{2}; \frac{1}{2}; \xi) - \frac{10}{9} {}_1F_1(-\frac{1}{2}; \frac{3}{2}; \xi)]}. \quad (55)$$

These are shown in Fig. 7; evidently, the hypothesis of OGE dominance of these decays can indeed be rejected, because the OGE decay mechanism predicts D/S amplitude ratios of the wrong sign for both $a_1 \rightarrow \rho\pi$ and $b_1 \rightarrow \omega\pi$.

Of course both sKs and OGE decay amplitudes actually are present in the physical decays, and Fig. 5 shows that the OGE contributions are not negligible here. It is especially interesting to investigate the combined effect of sKs and OGE amplitudes, because it may be possible to identify the individual contributions through interference. In the following we set $M(a_1) = M(b_1) = 1.23$ GeV and $M(\rho) = M(\omega) = 0.78$ GeV to remove small phase space effects. First in Fig. 8 we show the D/S ratio in $b_1 \rightarrow \omega\pi$ as a function of the OGE coupling strength α_s , for a realistic sKs amplitude ($b = 0.18$ GeV²), for several values of the wave function scale β . Evidently, the effect of OGE is to reduce D/S somewhat, and for the conventional $\alpha_s = 0.6$ this leads to a more realistic value of the wave function scale, $\beta \approx 0.35$ GeV. Recall that a rather large $\beta \approx 0.45$ GeV was required to fit the observed b_1 and a_1 D/S ratios with the sKs interaction treated in isolation.

A more definitive test of the presence of OGE contributions involves the ratio of a_1/b_1 D/S ratios; this is exactly $-1/2$ (assuming identical phase space and spatial wave functions) for any sKs or 3P_0 decay strength. We show this ratio versus the OGE coupling in Fig. 9, for the same parameter set as Fig. 8. For $\alpha_s = 0.6$ we expect a reduction in the a_1/b_1 D/S ratio to ≈ -0.46 to -0.47 . The current experimental ratio of $-0.35(9)$ suggests a larger departure from the sKs and 3P_0 prediction of $-1/2$, but is consistent with

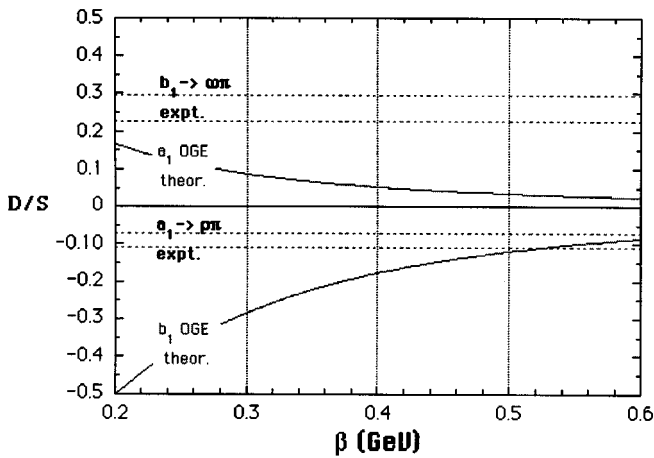


FIG. 7. D/S ratios in $b_1 \rightarrow \omega\pi$ and $a_1 \rightarrow \rho\pi$ assuming pure OGE decay amplitudes.

either theoretical result within errors. A more accurate experimental determination of these D/S ratios would be interesting as a test of the expected OGE corrections to nonperturbative sKs or 3P_0 decay amplitudes.

IV. SUMMARY AND CONCLUSIONS

In this paper we have discussed the current theoretical understanding of open flavor strong decays and proposed new “microscopic” quark and gluon mechanisms for these decays. We began by reviewing the 3P_0 decay model and introduced a diagrammatic representation for its decay amplitudes. We then carried out detailed calculations of the decay amplitudes for a representative set of light meson decays, first in the 3P_0 model and then in microscopic decay models, which assume that the $q\bar{q}$ pair is created by an OGE mechanism or by nonperturbative pair production from the scalar confining potential. These results were derived analytically using well-established light quark interactions and SHO wave functions.

We find that with conventional quark model parameters, the light $q\bar{q}$ open-flavor meson decays are usually dominated by $q\bar{q}$ pair production from the scalar confining potential. We refer to this as the sKs (scalar-kernel-scalar) decay model. This explains the success of the phenomenological 3P_0 decay model, since the $\bar{\psi}\psi$ scalar current produces pairs in a 3P_0 state, which is assumed *a priori* in the 3P_0 model. The dimensionless pair production strength γ is not determined theoretically in the 3P_0 model, and is treated as a free parameter. In contrast, in our calculations the absolute decay rates are completely determined by the $q\bar{q}$ wave function

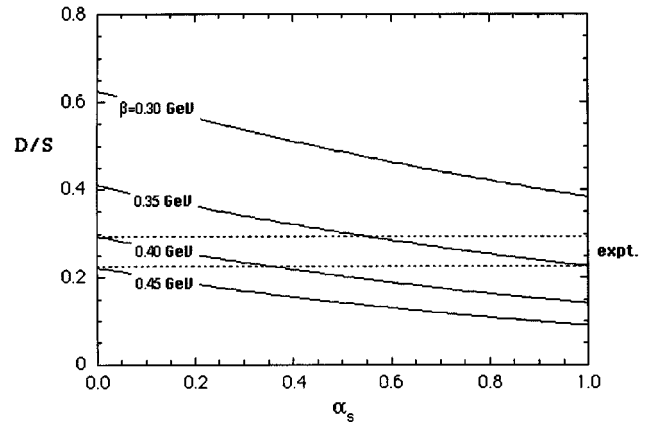


FIG. 8. D/S ratio in $b_1 \rightarrow \omega\pi$ with combined sKs and OGE decay amplitudes.

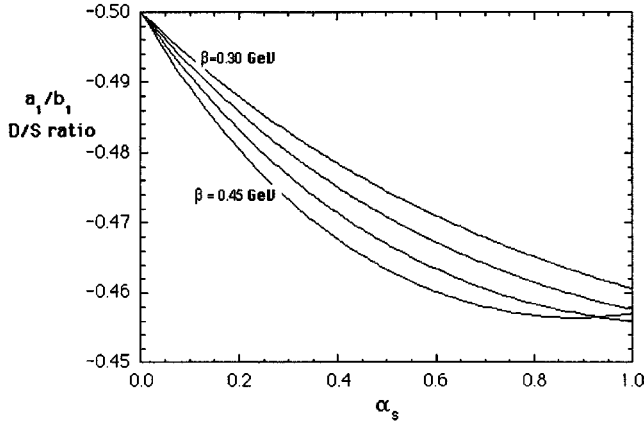


FIG. 9. The ratio of D/S ratios, $(a_1 \rightarrow \rho\pi)/(b_1 \rightarrow \omega\pi)$, with combined sKs and OGE decay amplitudes.

scale β and known QCD interaction parameters α_s , b (string tension), and m_q . In the sKs decay model, the 3P_0 strength γ corresponds approximately to the dimensionless combination $b/m_q\beta$.

Although there are differences in detail between the 3P_0 and sKs models due to the different overlap integrals, we find that the numerical predictions for relative decay rates and amplitudes in the decays we have considered are remarkably similar. In addition to explaining the success of the 3P_0 model, our description of decays also accounts naturally for the absence of ‘‘hairpin’’ diagrams; since the microscopic pair production interactions produce $q\bar{q}$ pairs in color-octet states, hairpin diagrams are forbidden without additional interactions. In the usual 3P_0 -like decay models, one assumes pair production of a $q\bar{q}$ color singlet, and hairpin diagrams are simply discarded without theoretical justification. Other tests of the color state of $q\bar{q}$ pair production in decays would be useful to discriminate between the 3P_0 model and our color-octet description.

We have seen that OGE $q\bar{q}$ pair production is usually dominated by nonperturbative sKs decay amplitudes, however there are numerically important OGE contributions in some channels, notably ${}^3P_0 \rightarrow {}^1S_0 + {}^1S_0$. In that case OGE pair production actually dominates the nonperturbative sKs amplitude, and insures broad $f_0(1300)$ and $K_0^*(1430)$ $q\bar{q}$ resonances. OGE pair production also makes characteristic contributions to some observables such as the D/S amplitude ratios in $b_1 \rightarrow \omega\pi$ and $a_1 \rightarrow \rho\pi$. It will be important to attempt to identify OGE contributions in these and similar multi-amplitude decays.

The general features of the sKs and 3P_0 decay models are very similar, and in a comparison that treats both pair production strengths b (in sKs) and γ (in 3P_0) as free parameters, there is no clear preference between these models in fitting the data. There is, however, a problem with the sKs model, because the string tension b has a preferred value of about 0.18 GeV^2 in meson spectroscopy; this gives decay amplitudes that are too large by about a factor of two. This discrepancy of scale may be due to the neglect of relativistic effects such as the m_q/E external line normalizations in Eq. (38). We suggest that future studies of decay amplitudes might search for evidence of OGE contributions, which differ considerably from sKs and 3P_0 amplitudes and may

dominate in certain channels such as ${}^3P_0 \rightarrow {}^1S_0 + {}^1S_0$.

It is clearly important to compare these hadron decay models to experiment over as wide a range of masses and length scales as possible. Thus, it would be interesting to apply these microscopic decay calculations to charmonium (where the transverse OGE contribution should be much smaller) and to strong decays of light baryons, for which new data is expected from the TJNAF experimental program. The simple exercise of extending these light meson calculations to higher- $L_{q\bar{q}}$ initial mesons also would be very useful, as it appears likely that large departures from 3P_0 (and sKs) model predictions due to OGE contributions could be found among the many decay channels available to these states.

ACKNOWLEDGMENTS

We would like to acknowledge useful communications with W. Bardeen, A. A. N. Barnes, H. Blundell, D.V. Bugg, S. Capstick, F.E. Close, E. Eichten, P. Geiger, S. Godfrey, N. Isgur, A. LeYaouanc, Z.P. Li, D. Lichtenberg, P.R. Page, O. Pene, J.M. Richard, W. Roberts, J. Rosner, and N. Törnqvist. We also acknowledge the support of J. Beene of the ORNL Physics Division. This research was sponsored in part by the United States Department of Energy under Contract No. DE-FG02-96ER40944 at North Carolina State University and Contract No. DE-AC05-96OR22464 managed by Lockheed Martin Energy Research Corp. at Oak Ridge National Laboratory.

APPENDIX A: DIAGRAMMATIC FORMULATION OF THE 3P_0 MODEL

1. General results

One may simplify calculations of decay amplitudes in the 3P_0 model by developing a diagrammatic description. This is nonessential for 3P_0 model calculations of meson decays since there are only two diagrams, but in our generalized decay models there are four diagrams, and it is useful to distinguish their contributions to prove relations between them. We anticipate that the diagrammatic description also will be useful in the more complicated combinatorics of baryon decays.

We begin by noting that the pair production component of the 3P_0 Hamiltonian (2) can be written in terms of creation operators as

$$H_I = \sum_{s\bar{s}} \int d^3k g \frac{m_q}{E_k} [\bar{u}_{\vec{k}s} v_{-\vec{k}\bar{s}}] b_{\vec{k}s}^\dagger d_{-\vec{k}\bar{s}}^\dagger. \quad (\text{A1})$$

We associate both the coupling constant g and the external-line spinor bilinear $(m_q/E_k)[\bar{u}_{\vec{k}s} v_{-\vec{k}\bar{s}}]$ with an effective 3P_0 $q\bar{q}$ pair production vertex. There is no additional factor of $-i$, unlike conventional field theoretic Feynman rules, because we are determining the matrix element of H_I instead of the T matrix.

We assume nonrelativistic $q\bar{q}$ wave functions for the initial and final mesons; in our notation a meson state is of the form

$$|A\rangle = \int d^3a \int d^3\bar{a} \phi(\vec{a} - \vec{\bar{a}}) \delta(\vec{A} - \vec{a} - \vec{\bar{a}}) |a\bar{a}\rangle \quad (\text{A2})$$

with implicit spin and flavor wave functions that are the usual nonrelativistic quark model forms. [For details of our conventions for the wave functions, see Ref. [14] and Appendix A; note that a factor of $1/(2\pi)^{3/2}$ was omitted inadvertently from the normalization of the wave function in Eq. (A15) in that reference.]

One now may evaluate the Hamiltonian matrix element for the decay $A \rightarrow BC$ in terms of straightforward overlap integrals. Schematically, we have a matrix element of the type

$$\langle b\bar{b}c\bar{c} | b_{\vec{k}s}^\dagger d_{-\vec{k}\bar{s}}^\dagger | a\bar{a} \rangle, \quad (\text{A3})$$

and it is useful to distinguish two Feynman diagrams (Fig. 10), which we refer to as d_1 if the produced quark goes into meson B and d_2 if it goes into C .

These are drawn so the ordered quark and antiquark content of the state can be read from the diagram by drawing a vertical line through it. Thus, in d_1 the initial state is $|A\rangle = |a\bar{a}\rangle$, but immediately after the pair creation we have $b_q^\dagger d_q^\dagger |a\bar{a}\rangle = |q\bar{q}a\bar{a}\rangle$. This is then rearranged to $|q\bar{a}a\bar{q}\rangle$

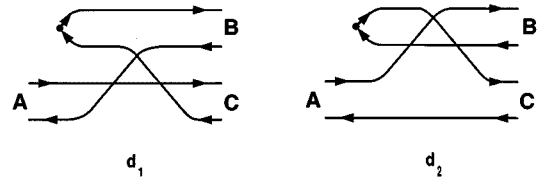


FIG. 10. $q\bar{q}$ meson decay diagrams in the 3P_0 decay model.

which is projected onto the final state $|BC\rangle = |b\bar{b}c\bar{c}\rangle$. The odd number of crossed lines in each diagram implies a (-1) phase (the ‘signature’ of the matrix element) due to permutation of quark and antiquark operators.

Specializing to diagram d_1 , the associated matrix element is of the form

$$\langle BC | H_I | A \rangle_{d_1} = I_{\text{signature}} I_{\text{flavor}} \mathbf{I}_{\text{spin+space}}. \quad (\text{A4})$$

The spatial overlap integral associated with diagram d_1 [before the spin matrix element is taken, which gives $\mathbf{I}_{\text{spin+space}}(d_1)$] is

$$\begin{aligned} \mathbf{I}_{\text{space}}(d_1) = & \int \int \int \int \int \int d^3a d^3\bar{a} d^3b d^3\bar{b} d^3c d^3\bar{c} \\ & \underbrace{\phi(\vec{a}-\vec{a}) \delta(\vec{A}-\vec{a}-\vec{a})}_{\text{meson A}} \underbrace{\phi^*(\vec{b}-\vec{b}) \delta(\vec{B}-\vec{b}-\vec{b})}_{\text{meson B}} \underbrace{\phi^*(\vec{c}-\vec{c}) \delta(\vec{C}-\vec{c}-\vec{c})}_{\text{meson C}} \\ & \underbrace{\int d^3k g \frac{m_q}{E_k} [\bar{u}_{\vec{k}s} v_{-\vec{k}\bar{s}}] \delta(\vec{k}-\vec{b}) \delta(-\vec{k}-\vec{c})}_{\text{pair production amplitude}} \underbrace{\delta(\vec{a}-\vec{c}) \delta(\vec{a}-\vec{b})}_{\text{spectator lines}} \end{aligned} \quad (\text{A5})$$

This result can be read directly from the diagram (see Fig. 11), using the pair production vertex (A1) and the fact that each unscattered ‘spectator’ line gives a factor of $\delta(\vec{k}_i - \vec{k}_f)$.

Thus the decay amplitude is a 21-dimensional integral involving 21 one-dimensional Δ functions. Only 18 of the integrations can be carried out trivially, which leaves a three-dimensional overlap integral times a $\delta(\vec{A}-\vec{B}-\vec{C})$ momentum-conserving Δ function,

$$\mathbf{I}_{\text{space}} = I_{\text{space}} \delta(\vec{A}-\vec{B}-\vec{C}), \quad (\text{A6})$$

as in Eq. (4). These overlap integrals are explicitly (setting $\vec{A}=0$ and $\vec{B}=-\vec{C}$)

$$\begin{aligned} I_{\text{space}}(d_1) = & \int d^3k \phi_A(2\vec{k}-2\vec{B}) \phi_B^*(2\vec{k}-\vec{B}) \\ & \times \phi_C^*(2\vec{k}-\vec{B}) \cdot g \frac{m_q}{E_k} [\bar{u}_{\vec{k}s_b} v_{-\vec{k}s_c}], \end{aligned} \quad (\text{A7})$$

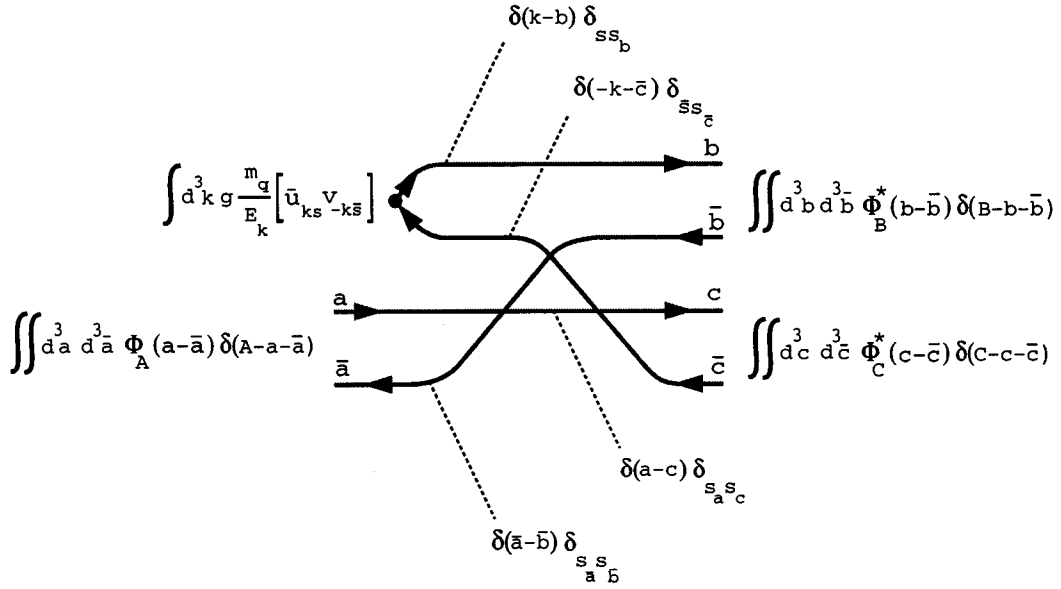
$$\begin{aligned} I_{\text{space}}(d_2) = & \int d^3k \phi_A(2\vec{k}+2\vec{B}) \phi_B^*(2\vec{k}+\vec{B}) \\ & \times \phi_C^*(2\vec{k}+\vec{B}) \cdot g \frac{m_q}{E_k} [\bar{u}_{\vec{k}s_c} v_{-\vec{k}s_b}]. \end{aligned} \quad (\text{A8})$$

The spin factor and labels $s_q, s_{\bar{q}}$ in these overlaps depend on the reaction being considered, and are determined by the external line labels attached to the diagrams, as illustrated below.

2. An illustrative 3P_0 decay: $\rho \rightarrow \pi\pi$

Here and in Appendix C we will use the decay $\rho^+(+\hat{z}) \rightarrow \pi^+\pi^0$ to illustrate our techniques, and simply quote results for other cases in the text. For this decay the flavor states are $|\rho^+\rangle = |\pi^+\rangle = -|u\bar{d}\rangle$ and $|\pi^0\rangle = (|u\bar{u}\rangle - |d\bar{d}\rangle)/\sqrt{2}$. Figure 12 shows the evaluation of the flavor factor for diagram d_1 .

The flavor factors of other decays can be determined similarly, and are tabulated below. For a given decay, such as

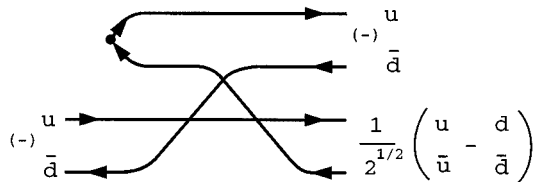
FIG. 11. Determination of the spatial overlap integral for diagram d_1 .

$f_2 \rightarrow \pi\pi$, we give the flavor weight factor for each diagram in a specific charge channel (in this case $f_2 \rightarrow \pi^+ \pi^-$). The resulting decay rate for $f_2 \rightarrow \pi^+ \pi^-$ then must be multiplied by a multiplicity factor \mathcal{F} to sum over all final flavor states (here $\mathcal{F}=3/2$ for $\pi^+ \pi^-$ and $\pi^0 \pi^0$). The ‘‘flavorless’’ decay amplitudes quoted in the text, Eqs. (7)–(15) and Eqs. (40)–(48), correspond to unit flavor factors, $I_{\text{flavor}}(d_1)=+1$ and $I_{\text{flavor}}(d_2)=\pm 1$. (The sign is chosen so the contributions of d_1 and d_2 add rather than cancel.) To convert these to physical decay amplitudes, one should multiply \mathcal{M}_{LS} in Eq. (7) or Eq. (40) by $I_{\text{flavor}}(d_i)$ from Table II, and multiply the resulting total decay rate by \mathcal{F} . The K^* is a special case because only one diagram contributes; in this case \mathcal{M}_{LS} should instead be multiplied by $I_{\text{flavor}}(d_1)/2$.

The spin states are $|\rho(+\hat{z})\rangle = |\uparrow\uparrow\rangle$ and $|\pi\rangle = (|\uparrow\downarrow\rangle - |\downarrow\uparrow\rangle)/\sqrt{2}$; taking the spin matrix element analogously to Fig. 12, we find a spin factor of $[(-1/2)\bar{u}_{\vec{k},\downarrow} v_{-\vec{k},\downarrow}]$ for this diagram. Combining these results and using the explicit Dirac spinor matrix element in Appendix B, we find

$$h_{fi}(d_1) = \underbrace{I_{\text{signature}}}_{(-1)} \underbrace{I_{\text{flavor}}}_{(+1/\sqrt{2})} I_{\text{spin+space}}(d_1), \quad (\text{A9})$$

where

FIG. 12. Determination of the flavor factor of $+1/\sqrt{2}$ for diagram d_1 in $\rho^+ \rightarrow \pi^+ \pi^0$.

$$I_{\text{spin+space}}(d_1) = -\frac{1}{2} g \int d^3k \phi_A(2\vec{k}-2\vec{B}) \times \phi_B^*(2\vec{k}-\vec{B}) \phi_C^*(2\vec{k}-\vec{B}) \frac{(k_x + ik_y)}{E_k}. \quad (\text{A10})$$

The second diagram d_2 has an opposite flavor factor, so the full result is

$$h_{fi} = -\frac{1}{\sqrt{2}} (I_{\text{spin+space}}(d_1) - I_{\text{spin+space}}(d_2)). \quad (\text{A11})$$

Since the overlap integrals satisfy $I(d_2, -\vec{B}) = +I(d_1, \vec{B})$, h_{fi} is odd under $\Omega_B \rightarrow -\Omega_B$, and can be written as

$$h_{fi} = -\sqrt{2} I_{\text{spin+space}}(d_1) = +\frac{1}{\sqrt{2}} \frac{g}{m_q} \int d^3k \times \phi_A(2\vec{k}-2\vec{B}) \phi_B^*(2\vec{k}-\vec{B}) \phi_C^*(2\vec{k}-\vec{B}) (k_x + ik_y). \quad (\text{A12})$$

We also have substituted m_q for E_k in Eq. (A10) to recover the nonrelativistic limit, which gives the 3P_0 model.

TABLE II. Flavor weight factors.

Generic decay	Subprocess	$I_{\text{flavor}}(d_1)$	$I_{\text{flavor}}(d_2)$	\mathcal{F}
$\rho \rightarrow \pi\pi$	$\rho^+ \rightarrow \pi^+ \pi^0$	$+1/\sqrt{2}$	$-1/\sqrt{2}$	1
$f \rightarrow \pi\pi$	$f \rightarrow \pi^+ \pi^-$	$-1/\sqrt{2}$	$-1/\sqrt{2}$	3/2
$a \rightarrow \rho\pi$	$a^+ \rightarrow \rho^+ \pi^0$	$+1/\sqrt{2}$	$-1/\sqrt{2}$	2
$b \rightarrow \omega\pi$	$b^+ \rightarrow \omega \pi^+$	$+1/\sqrt{2}$	$+1/\sqrt{2}$	1
$h \rightarrow \rho\pi$	$h \rightarrow \rho^+ \pi^-$	$-1/\sqrt{2}$	$-1/\sqrt{2}$	3
$K^* \rightarrow K\pi$	$K^{*+} \rightarrow K^+ \pi^0$	$+1/\sqrt{2}$	0	3

Frequently in the literature these decay amplitudes are evaluated using SHO $q\bar{q}$ wave functions, which lead to closed-form results. For $L_{q\bar{q}}=0$ mesons, our Gaussian momentum space wave function $\phi(\vec{k}_q - \vec{k}_{\bar{q}})$, with $\vec{k} = \vec{k}_q = -\vec{k}_{\bar{q}}$, is

$$\phi(2\vec{k}) = \frac{1}{\pi^{3/4}\beta^{3/2}} e^{-k^2/2\beta^2}. \quad (\text{A13})$$

We note in passing that the $L_{q\bar{q}}=1$ wave function used in this paper is

$$\phi_{1m}(2\vec{k}) = \frac{2^{3/2}}{3^{1/2}} \frac{1}{\pi^{1/4}\beta^{3/2}} \frac{k}{\beta} e^{-k^2/2\beta^2} Y_{1m}(\Omega_k). \quad (\text{A14})$$

On substitution into Eq. (A12), $\phi(2\vec{k})$ gives a $\rho^+(+\hat{z}) \rightarrow \pi^+ \pi^0$ decay amplitude of

$$h_{fi} = -\frac{2^{7/2}}{3^3} \pi^{-1/4} \frac{g}{m_q} \frac{P}{\beta^{3/2}} e^{-P^2/12\beta^2} Y_{11}(\Omega_B) \quad (\text{A15})$$

and an $\mathcal{M}_{10}^{\rho^+ \rightarrow \pi^+ \pi^0}$ amplitude of

$$\mathcal{M}_{10}^{\rho^+ \rightarrow \pi^+ \pi^0} = -\frac{2^{9/2}}{3^3} \frac{1}{\pi^{1/4}\beta^{1/2}} \frac{g}{2m_q} \frac{P}{\beta} e^{-P^2/12\beta^2} Y_{11}(\Omega_B). \quad (\text{A16})$$

Substitution into Eq. (6) then gives the total decay rate

$$\Gamma_{\rho \rightarrow \pi\pi} = \pi^{1/2} \left(\frac{2^{10}}{3^6} \right) \left(\frac{g}{2m_q} \right)^2 M_\rho (P/\beta)^3 e^{-P^2/6\beta^2}, \quad (\text{A17})$$

which with the identification $\gamma = g/2m_q$ is the usual 3P_0 result.

Many features of this decay rate could be anticipated on general grounds. Specifically, (1) the $(g/m_q)^2$ dependence follows from the $O(g)$ of the amplitude and the nonrelativistic limit of Eq. (2), (2) the factor of M_ρ comes from phase space and the relation $E_B E_C / M_A = M_\rho/4$, (3) the P^3 threshold dependence is expected for a P -wave final state, (4) dimensional arguments then require a factor of $1/\beta^3$, and (5) an exponential in $(P/\beta)^2$ is expected given SHO wave functions.

Only the overall numerical coefficient and the factor of $1/6$ in the exponential (present in all 3P_0 SHO $A \rightarrow BC$ $q\bar{q}$ meson decays) require detailed calculation.

APPENDIX B: OVERLAP INTEGRALS AND SPIN FACTORS

In the text we discussed the evaluation of only one of the four decay diagrams present in $A \rightarrow BC$ meson decay in JKJ models. Here we give the overlap integrals associated with all four diagrams:

$$\begin{aligned} I_{\text{space}}(d_{1q}) = & + \frac{1}{(2\pi)^3} \iint d^3a d^3c \phi_A(2\vec{a}) \\ & \times \phi_B^*(2\vec{a} + \vec{B}) \phi_C^*(2\vec{c} + \vec{B}) [\bar{u}_{b_s b} \Gamma v_{\bar{c}_s \bar{c}}] \\ & \times \mathcal{K}(\vec{a} - \vec{c}) [\bar{u}_{c_s c} \Gamma u_{a_s a}] \end{aligned} \quad (\text{B1})$$

(with implicit momentum constraints specific to this diagram of $\vec{b} = \vec{a} + \vec{B}$ and $\vec{c} = -\vec{B} - \vec{c}$),

$$\begin{aligned} I_{\text{space}}(d_{1\bar{q}}) = & - \frac{1}{(2\pi)^3} \iint d^3a d^3b \phi_A(2\vec{a}) \\ & \times \phi_B^*(2\vec{b} - \vec{B}) \phi_C^*(2\vec{a} + \vec{B}) [\bar{v}_{b_s b} \Gamma v_{\bar{c}_s \bar{c}}] \\ & \times \mathcal{K}(\vec{a} - \vec{b}) [\bar{v}_{\bar{a}_s a} \Gamma v_{\bar{b}_s b}] \end{aligned} \quad (\text{B2})$$

(with $\vec{c} = -\vec{B} - \vec{c}$, $\vec{a} = -\vec{a}$, and $\vec{b} = \vec{B} - \vec{b}$),

$$\begin{aligned} I_{\text{space}}(d_{2q}) = & + \frac{1}{(2\pi)^3} \iint d^3a d^3b \phi_A(2\vec{a}) \\ & \times \phi_B^*(2\vec{b} - \vec{B}) \phi_C^*(2\vec{a} - \vec{B}) [\bar{u}_{c_s c} \Gamma v_{\bar{b}_s b}] \\ & \times \mathcal{K}(\vec{a} - \vec{b}) [\bar{u}_{b_s b} \Gamma u_{a_s a}] \end{aligned} \quad (\text{B3})$$

(with $\vec{c} = \vec{a} - \vec{B}$ and $\vec{b} = \vec{B} - \vec{b}$),

$$\begin{aligned} I_{\text{space}}(d_{2\bar{q}}) = & - \frac{1}{(2\pi)^3} \iint d^3a d^3c \phi_A(2\vec{a}) \\ & \times \phi_B^*(2\vec{a} - \vec{B}) \phi_C^*(2\vec{c} + \vec{B}) [\bar{u}_{c_s c} \Gamma v_{\bar{b}_s b}] \\ & \times \mathcal{K}(\vec{a} - \vec{c}) [\bar{v}_{\bar{a}_s a} \Gamma v_{\bar{c}_s c}] \end{aligned} \quad (\text{B4})$$

(with $\vec{a} = -\vec{a}$, $\vec{b} = \vec{B} - \vec{a}$, and $\vec{c} = -\vec{B} - \vec{c}$).

In our evaluation of decay matrix elements in JKJ models, we also require spin matrix elements, which involve the nonrelativistic $O(p/m)$ matrix elements of Dirac bilinears with $\Gamma = \gamma^0$, $\vec{\gamma}$, and I and Pauli spin matrix elements. These are

$$\lim_{v/c \rightarrow 0} [\bar{u}_{q's'} \Gamma u_{qs}] = \begin{cases} \delta_{ss'} & \Gamma = \gamma^0, \\ \frac{1}{2m_q} [(\vec{q} + \vec{q}') \delta_{ss'} - i \langle s' | \vec{\sigma} | s \rangle \times (\vec{q}' - \vec{q})] & \Gamma = \vec{\gamma}, \\ \delta_{ss'} & \Gamma = \text{I}, \end{cases} \quad (\text{B5})$$

$$\lim_{v/c \rightarrow 0} [\bar{u}_{qs} \Gamma v_{\bar{q}\bar{s}}] = \begin{cases} \frac{1}{2m_q} \langle s\bar{s} | \vec{\sigma} | 0 \rangle \cdot (\vec{q} + \vec{q}) & \Gamma = \gamma^0, \\ \langle s\bar{s} | \vec{\sigma} | 0 \rangle & \Gamma = \vec{\gamma}, \\ \frac{1}{2m_q} \langle s\bar{s} | \vec{\sigma} | 0 \rangle \cdot (\vec{q} - \vec{q}) & \Gamma = \mathbf{I}, \end{cases} \quad (\text{B6})$$

$$\lim_{v/c \rightarrow 0} [\bar{v}_{\bar{q}\bar{s}} \Gamma v_{\bar{q}'\bar{s}'}] = \begin{cases} \delta_{\bar{s}\bar{s}'} & \Gamma = \gamma^0, \\ \frac{1}{2m_q} [(\vec{q} + \vec{q}') \delta_{\bar{s}\bar{s}'} - i \langle \bar{s}' | \vec{\sigma} | \bar{s} \rangle \times (\vec{q}' - \vec{q})] & \Gamma = \vec{\gamma}, \\ -\delta_{\bar{s}\bar{s}'} & \Gamma = \mathbf{I}. \end{cases} \quad (\text{B7})$$

The explicit scattering and pair-production matrix elements of Pauli spinors, in terms of the spherical basis vectors $\hat{e}_{\pm} = \mp(\hat{x} \pm i\hat{y})/\sqrt{2}$ and $\hat{e}_0 = \hat{z}$, are

$$\langle \uparrow | \vec{\sigma} | \uparrow \rangle = -\langle \downarrow | \vec{\sigma} | \downarrow \rangle = \hat{e}_0, \quad (\text{B8})$$

$$\langle \uparrow | \vec{\sigma} | \downarrow \rangle = \sqrt{2} \hat{e}_-, \quad (\text{B9})$$

$$\langle \downarrow | \vec{\sigma} | \uparrow \rangle = -\sqrt{2} \hat{e}_+, \quad (\text{B10})$$

$$\langle \uparrow | \vec{\sigma} | \uparrow \rangle = -\langle \downarrow | \vec{\sigma} | \downarrow \rangle = -\hat{e}_0, \quad (\text{B11})$$

$$\langle \uparrow | \vec{\sigma} | \downarrow \rangle = \sqrt{2} \hat{e}_+, \quad (\text{B12})$$

$$\langle \downarrow | \vec{\sigma} | \uparrow \rangle = -\sqrt{2} \hat{e}_-, \quad (\text{B13})$$

$$\langle \uparrow \uparrow | \vec{\sigma} | 0 \rangle = \sqrt{2} \hat{e}_-, \quad (\text{B14})$$

$$\langle \uparrow \downarrow | \vec{\sigma} | 0 \rangle = \langle \downarrow \uparrow | \vec{\sigma} | 0 \rangle = -\hat{e}_0, \quad (\text{B15})$$

$$\langle \downarrow \downarrow | \vec{\sigma} | 0 \rangle = \sqrt{2} \hat{e}_+. \quad (\text{B16})$$

APPENDIX C: $\rho \rightarrow \pi\pi$ IN JKJ DECAY MODELS

We will illustrate a JKJ decay calculation in detail using the reaction $\rho^+(+\hat{z}) \rightarrow \pi^+ \pi^0$, as in our discussion of the 3P_0 model in Appendix A. We will evaluate the $\rho \rightarrow \pi\pi$ decay rate using the $j^0 K j^0$ interaction in Eqs. (27)–(29), and simply quote results in the text for the other cases. For each type of JKJ interaction, we find that the four diagrams give equal contributions to this decay, so we discuss only diagram d_{1q} (Fig. 13).

For all the JKJ interactions, this diagram has a signature of (-1) , a color factor of $+2^2/3^{3/2}$, and a flavor factor (for $\rho^+ \rightarrow \pi^+ \pi^0$) of $+1/2^{1/2}$. Differences in the relative importance of the decay mechanisms arise in the spin-space overlap integrals and the Γ spinor matrix elements.

In the text we derived the spatial overlap integral for diagram d_{1q} in the nonrelativistic limit, Eq. (39):

$$I_{\text{space}}(d_{1q}) = \frac{1}{(2\pi)^3} \int \int d^3a d^3c \phi_A(2\vec{a}) \phi_B^*(2\vec{a} + \vec{B}) \\ \times \phi_C^*(2\vec{c} + \vec{B}) [\bar{u}_{bs_b} \Gamma v_{\bar{c}s_{\bar{c}}}] \mathcal{K}(|\vec{a} - \vec{c}|) \\ \times [\bar{u}_{cs_c} \Gamma u_{as_a}]. \quad (\text{C1})$$

To evaluate this for $\rho^+(+\hat{z}) \rightarrow \pi^+ \pi^0$, note that for the color Coulomb interaction ($\Gamma = \gamma^0$) the spinor bilinears are

$$[\bar{u}_{bs_b} \gamma^0 v_{\bar{c}s_{\bar{c}}}] [\bar{u}_{cs_c} \gamma^0 u_{as_a}] = \frac{1}{2m_q} \langle s_b s_c | \vec{\sigma} | 0 \rangle (\vec{b} + \vec{c}) \delta_{s_c s_a}. \quad (\text{C2})$$

Attaching the spin wave functions to the diagram d_{1q} gives an overall factor of $(-1/2)$ and sets $s_b = \downarrow$ and $s_{\bar{c}} = \bar{\downarrow}$, so the spin matrix element is $\langle \vec{\sigma} \rangle_{q\bar{q}} = (-1/2) \langle \downarrow \bar{\downarrow} | \vec{\sigma} | 0 \rangle = -\hat{e}_+ / \sqrt{2}$. With the substitutions $\vec{Q} = (\vec{a} - \vec{c}) = (\vec{b} + \vec{c})$ and $\vec{\Sigma} = (\vec{a} + \vec{c})/2$, h_{fi} becomes

$$h_{fi}(d_{1q}) = \underbrace{(-1)}_{\text{signature}} \underbrace{\left(+ \frac{2^2}{3^{3/2}} \right)}_{\text{color}} \underbrace{\left(+ \frac{1}{2^{1/2}} \right)}_{\text{flavor}} \\ \times \int \int \frac{d^3Q d^3\Sigma}{(2\pi)^3} \frac{\langle \vec{\sigma} \rangle_{q\bar{q}} \cdot \vec{Q}}{2m_q} \mathcal{K}(Q) \phi_\rho(2\vec{\Sigma} + \vec{Q}) \\ \times \phi_{\pi^+}^*(2\vec{\Sigma} + \vec{Q} + \vec{B}) \phi_{\pi^0}^*(2\vec{\Sigma} - \vec{Q} + \vec{B}). \quad (\text{C3})$$

Without additional information about the spatial wave functions this is the final result. To proceed we assume standard quark model Gaussian wave functions (A13) for the mesons.

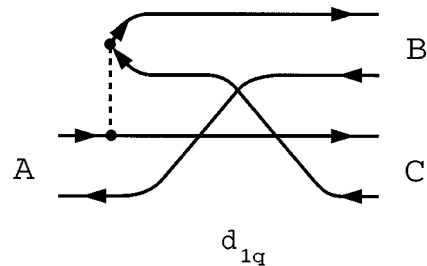


FIG. 13. Decay diagram d_{1q} .

The $d^3\Sigma$ integral then can be carried out, which gives

$$h_{fi}(d_{1q}) = -2^{-1}3^{-3}\pi^{-15/4}m_q^{-1}\beta^{-3/2}e^{-x^2/16} \times \underbrace{\int d^3Q \langle \vec{\sigma} \rangle_{q\bar{q}} \cdot \vec{Q} \mathcal{K}(Q) \exp\left\{-\frac{1}{3\beta^2}\left(\vec{Q}-\frac{1}{4}\vec{B}\right)^2\right\}}_I, \quad (C4)$$

where we have again abbreviated $P/\beta = x$.

We may evaluate this intermediate integral I by returning to coordinate space using Eq. (37) and integrating over d^3Q , which gives

$$I = 3^{3/2}\pi^{3/2}\beta^3 \int d^3r \langle \vec{\sigma} \rangle_{q\bar{q}} \cdot \left(\frac{1}{4}\vec{B} + \frac{3i}{2}\beta^2\vec{r}\right) \times K(r) e^{i\vec{B}\cdot\vec{r}/4} e^{-3\beta^2r^2/4}. \quad (C5)$$

For $\langle \vec{\sigma} \rangle_{q\bar{q}}$ in this reaction we have

$$\langle \vec{\sigma} \rangle_{q\bar{q}} \cdot \vec{r} = -\sqrt{\frac{2\pi}{3}}rY_{11}(\Omega), \quad (C6)$$

and the angular integrals can then be carried out using a spherical harmonic expansion of the plane wave in Eq. (C5). This gives

$$I = -2^{5/2}3\pi^3\beta^3Y_{11}(\Omega_B) \int_0^\infty r^2 dr K(r) e^{-3\beta^2r^2/4} \times \left[\frac{1}{4}Pj_0(Pr/4) - \frac{3}{2}\beta^2rj_1(Pr/4)\right]. \quad (C7)$$

Since the kernel is simply $K(r) = \alpha_s/r$ in this case, the radial integrals can be evaluated in terms of confluent hypergeometric functions using the general formula

$$\int_0^\infty dr r^n j_\ell(ar) e^{-br^2} = \sqrt{\pi} \frac{a^\ell}{b^\phi} \frac{\Gamma(\phi)}{2^{\ell+2}\Gamma(\ell+3/2)} \times {}_1F_1\left(\frac{\ell-n}{2}+1; \ell+\frac{3}{2}; \frac{a^2}{4b}\right) e^{-a^2/4b}, \quad (C8)$$

where $\phi = (n + \ell + 1)/2$. This result suffices for all the overlap integrals we encounter in JKJ decay models with SHO wave functions and power-law kernels.

Applied to the Coulomb case, our result for the integral I is

$$I = -2^{3/2}\pi^3\alpha_s\beta^2x \left[{}_1F_1\left(\frac{1}{2}; \frac{3}{2}; \xi\right) - \frac{2}{3} {}_1F_1\left(\frac{1}{2}; \frac{5}{2}; \xi\right) \right] e^{-x^2/48} Y_{11}(\Omega_B), \quad (C9)$$

where $\xi = x^2/48$. Using this integral, we obtain our final result for diagram d_{1q} ,

$$h_{fi}(d_{1q}) = \frac{2^{1/2}}{3^3} \pi^{-3/4} \frac{\alpha_s}{m_q} \beta^{1/2} x \left[{}_1F_1\left(\frac{1}{2}; \frac{3}{2}; \xi\right) - \frac{2}{3} {}_1F_1\left(\frac{1}{2}; \frac{5}{2}; \xi\right) \right] e^{-x^2/12} Y_{11}(\Omega_B). \quad (C10)$$

On multiplying by 4 for the four equivalent diagrams, we obtain the full result for h_{fi} for $\rho^+ (+\hat{z}) \rightarrow \pi^+ \pi^0$. We can abstract the $j^0 K j^0$ decay amplitude \mathcal{M}_{LS} in Eq. (6) from this; removing the $\rho^+ \rightarrow \pi^+ \pi^0$ flavor factor of $1/\sqrt{2}$, we have

$$\mathcal{M}_{10}^{(3S_1 \rightarrow 1S_0 + 1S_0)} = + \frac{2^3}{3^3} \pi^{-3/4} \frac{\alpha_s}{m_q} \beta^{1/2} x \left[{}_1F_1\left(\frac{1}{2}; \frac{3}{2}; \xi\right) - \frac{2}{3} {}_1F_1\left(\frac{1}{2}; \frac{5}{2}; \xi\right) \right] e^{-x^2/12}, \quad (C11)$$

which is equivalent to the result quoted in Eq. (41). Using Eq. (6), we find that the total $\rho \rightarrow \pi\pi$ decay rate due to color Coulomb OGE (treated in isolation) is

$$\Gamma_{\rho \rightarrow \pi\pi}^{j^0 K j^0} = \pi^{-1/2} \left(\frac{2^6}{3^6}\right) \alpha_s^2 \left(\frac{\beta}{m_q}\right)^2 \frac{E_\pi^2}{M_\rho} x^3 \left[{}_1F_1\left(\frac{1}{2}; \frac{3}{2}; \xi\right) - \frac{2}{3} {}_1F_1\left(\frac{1}{2}; \frac{5}{2}; \xi\right) \right]^2 e^{-x^2/6}. \quad (C12)$$

Alternatively, for the specific case of a Coulomb kernel we can evaluate the momentum space integral (C3) directly. The required integrals and others needed to evaluate decay amplitudes for P -wave quarkonia are given below.

$$\int q d^3Q (1/\vec{Q}^2) e^{-a(\vec{Q}-\vec{Q}_0)^2} = \frac{\pi^{3/2}}{a^{1/2}} \left[2 {}_1F_1\left(\frac{1}{2}, \frac{3}{2}, a\vec{Q}_0^2\right) \right] e^{-a\vec{Q}_0^2}, \quad (C13)$$

$$\int d^3Q (Q_i/\vec{Q}^2) e^{-a(\vec{Q}-\vec{Q}_0)^2} = \frac{\pi^{3/2}}{a^{1/2}} \left[\frac{2}{3} Q_{0i} {}_1F_1\left(\frac{3}{2}, \frac{5}{2}, a\vec{Q}_0^2\right) \right] e^{-a\vec{Q}_0^2}, \quad (C14)$$

$$\int d^3Q (Q_i Q_j/\vec{Q}^2) e^{-a(\vec{Q}-\vec{Q}_0)^2} = \frac{\pi^{3/2}}{a^{1/2}} \left[\frac{1}{3a} \delta_{ij} {}_1F_1\left(\frac{3}{2}, \frac{5}{2}, a\vec{Q}_0^2\right) + \frac{2}{5} Q_{0i} Q_{0j} {}_1F_1\left(\frac{5}{2}, \frac{7}{2}, a\vec{Q}_0^2\right) \right] e^{-a\vec{Q}_0^2}, \quad (C15)$$

$$\int d^3Q (Q_i Q_j/\vec{Q}^4) e^{-a(\vec{Q}-\vec{Q}_0)^2} = \frac{\pi^{3/2}}{a^{1/2}} \left[\frac{2}{3} \delta_{ij} {}_1F_1\left(\frac{1}{2}, \frac{5}{2}, a\vec{Q}_0^2\right) + \frac{4}{15} a Q_{0i} Q_{0j} {}_1F_1\left(\frac{3}{2}, \frac{7}{2}, a\vec{Q}_0^2\right) \right] e^{-a\vec{Q}_0^2}, \quad (C16)$$

$$\begin{aligned}
& \int d^3 Q (\mathcal{Q}_i \mathcal{Q}_j \mathcal{Q}_k / \vec{Q}^4) e^{-a(\vec{Q} - \vec{Q}_0)^2} \\
&= \frac{\pi^{3/2}}{a^{1/2}} \left[\frac{2}{15} (\delta_{ij} \mathcal{Q}_{0k} + \delta_{jk} \mathcal{Q}_{0i} + \delta_{ki} \mathcal{Q}_{0j}) {}_1F_1 \left(\frac{3}{2}, \frac{7}{2}, a \vec{Q}_0^2 \right) \right. \\
&\quad \left. + \frac{4}{35} a \mathcal{Q}_{0i} \mathcal{Q}_{0j} \mathcal{Q}_{0k} {}_1F_1 \left(\frac{5}{2}, \frac{9}{2}, a \vec{Q}_0^2 \right) \right] e^{-a \vec{Q}_0^2}. \quad (\text{C17})
\end{aligned}$$

This approach applied to $\rho \rightarrow \pi\pi$ leads to the result

$$\Gamma_{\rho \rightarrow \pi\pi}^{j^0 K_j^0} = \pi^{-1/2} \left(\frac{2^6}{3^8} \right) \alpha_s^2 \left(\frac{\beta}{m_q} \right)^2 \frac{E_\pi^2}{M_\rho} x^3 {}_1F_1 \left(\frac{3}{2}; \frac{5}{2}; \xi \right)^2 e^{-x^2/6}, \quad (\text{C18})$$

which is equivalent to Eq. (C12).

Relations between confluent hypergeometric functions with different indices allow these results to be written in various forms. We typically express our final results for decay amplitudes as linear combinations of confluent hypergeometric functions with constant coefficients and a common

first index a , times a centrifugal factor of $x^{L_{BC}}$. These rearrangements are straightforward using the recurrence relations

$$\begin{aligned}
{}_1F_1(a; c; x) &= \frac{(c-1)}{(a-1)} {}_1F_1(a-1; c-1; x) \\
&\quad + \frac{(a-c)}{(a-1)} {}_1F_1(a-1; c; x) \quad (\text{C19})
\end{aligned}$$

and

$$\begin{aligned}
x {}_1F_1(a; c; x) &= \frac{(c-1)(c-2)}{(a-1)} [{}_1F_1(a-1; c-2; x) \\
&\quad - {}_1F_1(a-1; c-1; x)]. \quad (\text{C20})
\end{aligned}$$

The decay rates due to transverse OGE and the confining interaction may be derived using the same techniques, with the minor complication that transverse OGE also has initial-line spin-flip contributions. These results are quoted in Sec. III D.

-
- [1] L. Micu, Nucl. Phys. **B10**, 521 (1969).
[2] A. Le Yaouanc, L. Oliver, O. Pène, and J. Raynal, Phys. Rev. D **8**, 2223 (1973); **9**, 1415 (1974); **11**, 1272 (1975).
[3] Since the literature is extensive, we cite only a few of the original and more recent references. For recent summaries of the 3P_0 and related decay models see H.G. Blundell and S. Godfrey, Phys. Rev. D **53**, 3700 (1996); P.R. Page, Ph.D. thesis, University of Oxford, 1995. For applications to charmonium see A. Le Yaouanc, L. Oliver, O. Pène, and J. Raynal, Phys. Lett. **71B**, 397 (1977); **72B** 57 (1977); P.R. Page, Nucl. Phys. **B446**, 189 (1995). For baryon decays, see S. Capstick and N. Isgur, Phys. Rev. D **34**, 2809 (1986), and [10].
[4] P. Geiger and E.S. Swanson, Phys. Rev. D **50**, 6855 (1994).
[5] R. Kokoski and N. Isgur, Phys. Rev. D **35**, 907 (1987).
[6] S. Godfrey and N. Isgur, Phys. Rev. D **32**, 189 (1985).
[7] J.W. Alcock, M.J. Burfitt, and W.N. Cottingham, Z. Phys. C **25**, 161 (1984); S. Kumano and V.R. Pandharipande, Phys. Rev. D **38**, 146 (1988).
[8] H.J. Schnitzer, Phys. Rev. Lett. **35**, 1540 (1975).
[9] C. Michael, Phys. Rev. Lett. **56**, 1219 (1986).
[10] S. Capstick and W. Roberts, Phys. Rev. D **49**, 4570 (1994).
[11] Particle Data Group, L. Montanet *et al.*, Phys. Rev. D **50**, 1173 (1994).
[12] ARGUS Collaboration, H. Albrecht *et al.*, Z. Phys. C **58**, 61 (1993).
[13] E. Eichten, K. Gottfried, T. Kinoshita, K.D. Lane, and T.M. Yan, Phys. Rev. D **17**, 3090 (1978); E. Eichten and J. Goldman, *ibid.* **23**, 203 (1981); see also W.S. Jaronski and D. Robson, *ibid.* **32**, 1198 (1985).
[14] T. Barnes and E.S. Swanson, Phys. Rev. D **46**, 131 (1992).